Draft version May 17, 2018
Typeset using LaTeX **twocolumn** style in AASTeX62

Do Lyα absorbers co-rotate with galaxy disks?

David M. French, Bart P. Wakker[1]

[1]*Department of Astronomy, University of Wisconsin, Madison, WI 53706, USA*

ABSTRACT

We present results of a study comparing the relative velocity of Lyα absorbers to the rotation direction and velocity of nearby galaxy disks. We find...

Keywords: galaxies:intergalactic medium, galaxies:evolution, galaxies:halos, quasars: absorption lines

1. INTRODUCTION

Our current ΛCDM cosmology picture describes galaxies forming hierarchically out of overdensities in the underlying dark matter distribution. Simulations predict

As matter is funneled toward a growing galaxy, simulations predict conservation of angular momentum redistributes the angular momentum in this gas to match that of the halo and underlying dark matter as the gas is shock-heated and slowly cools (Danovich et al. (2012), Shen et al. (2013)). As this infalling gas is responsible for birthing and continuing to feed the galaxies, it is expected that the extended gaseous halos should rotate in the same sense as both the galactic disks and dark matter halos.

Galaxy rotation curves have been observed to extend at constant velocity out to... (cite...). It becomes increasingly difficult to measure gas rotation much farther from this however as the density rapidly decreases. Within this region the galaxy disks transition into circumgalactic medium (CGM), and eventually the CGM merges with the intergalactic medium (IGM). At what point, however, does the surrounding medium cease to circulate with the galaxy?

Cosmological SPH simulations such as those by Stewart et al. (2011, 2013) **NEED MORE CURRENT ONES TOO** suggests that halo gas should co-rotate with disk-gas out to at least 100 kpc, and that absorption in intervening QSO sightlines should be able to accurately capture this rotation signature.

Observational confirmation has be inconclusive, however. Côté et al. 2005 probed the halos of nine galaxies using *HST* observed background QSOs, finding large warps would be needed to explain the velocity of H I absorbers by an extended rotating disk. Wakker & Savage (2009) compiled a sample of 4 galaxy-QSO systems from the literature, finding only 1/4 of Lyα absorbers appeared to co-rotate with the associated galaxy disk. Approaching the question from a different angle, Bowen et al. (2016) probed the halo of a single galaxy, NGC1097, with 4 nearby QSO sightlines, and suggests that an extended, slowly rotating disk with additional inflowing IGM material best matches observations.

Diamond-Stanic et al. (2016) detect co-rotating Hα emission and Mg II and Fe II absorption toward a Milky Way-like galaxy at $z = 0.413$.

Numerous studies have shown a correlation between equivalent width and decreasing velocity difference between galaxies and IGM absorbers (e.g., French & Wakker 2017, MORE).

To make progress here, we have obtained rotation curves for 12 nearby spiral galaxies which are located within 500 kpc of a background QSO observed by the Cosmic Origins Spectrograph (COS) on *HST*. A literature search yielded an additional 16 galaxies with published rotation curves and known orientations. Each of these is probed by at least one QSO within 500 kpc.

We have augmented this new sample with additional galaxies with known rotation velocity and orientation from the literature. In Section 2 we describe the selection and reduction of both SALT and COS spectra. We then discuss each galaxy-QSO system in detail in Section 3, and introduce our halo-velocity model for interpreting these systems in Section 4. In Section 5 we discuss the overall results of this exercise and present a physically-motivated interpretation of these results. See Section 6 for a summary of our results and conclusions.

2. DATA AND ANALYSIS

2.1. *SALT Data*

Our sample contains 12 galaxies observed with the Southern African Large Telescope (SALT) Robert Stobie Spectrograph (RSS) in longslit mode. These 12 were selected from a larger pool of 48 submitted targets by the SALT observing queue. These 48 possible targets were chosen for their proximity to background QSOs whose spectra contained promising Lyα lines. Finally, we only included galaxies with $z \leq 0.33$ ($cz \leq 10,000$ km s^{-1}), angular sizes less than 6' to enable easy sky subtraction without taking additional exposures, and surface brightnesses sufficient to keep exposure times below $\sim 1300s$. Table 1 summarizes these observations. Data was taken

for 2 additional galaxies, NGC3640 and NGC2962, but proved unusable due to issues with spectral identification and low signal-to-noise (respectively).

All SALT galaxy spectra were reduced and extracted using the standard PySALT reduction package (**CITATION**), which includes procedures to prepare the data, correct for gain, cross-talk, bias, and overscan, and finally mosaic the images from the 3 CCDs. Next, we rectify the images with wavelength solutions found via Ne and Ar arc lamp spectra line identification. Finally, we perform a basic sky subtraction using an off-sky portion of the spectrum, and extract 5-10 pixel wide 1-D strips from the reduced 2-D spectrum.

For each 1-D spectrum, we identify the Hα emission lines and perform a non-linear least-squares Voigt profile fit using the Python package LMFIT[1]. The line centroid and 1σ standard errors are returned, and these fits are then shifted to rest-velocity based on the galaxy systemic redshift and heliocentric velocity corrections are calculated with the IRAF rvcorrect procedure. The final rotation velocity is calculated by then applying the inclination correction, $v_{rot} = v/\sin(i)$. Final errors are calculated as a quadrature sum of 1σ fit errors, systemic redshift error, and inclination uncertainty as follows:

$$\sigma^2 = \left(\frac{\partial v_{rot}}{\partial \lambda_{obs}}\right)^2 (\Delta\lambda_{obs})^2 + \left(\frac{\partial v_{rot}}{\partial v_{sys}}\right)^2 (\Delta v_{sys})^2 + \left(\frac{\partial v_{rot}}{\partial i}\right)^2 (\Delta i)^2, \quad (1)$$

where $\Delta\lambda_{obs}$, Δv_{sys}, and Δi are the errors in observed line center, galaxy redshift, and inclination, respectively.

We determine the inclination error by calculating the standard deviation of the set of all axis ratio values available in NED for each galaxy. The final physical scale is calculated using the SALT image scale of 0.1267 arcsec/pixel, multiplied by the 4-pixel spatial binning, and converted to physical units using a redshift-independent distance if available, and a Hubble flow estimate if not. We adopt a Hubble constant of $H_0 = 71$ km s^{-1}Mpc^{-1} throughout.

Finally, we calculate our approaching and receding velocities via a weighted mean of the outer 1/2 of each rotation curve, with errors calculated as weighted standard errors in the mean. Our final redshifts are calculated by forcing symmetric rotation, such that the outer 1/2 average velocity for each side matches in magnitude. See Appendix A for rotation curves and slit-position charts for each observed galaxy.

[1] http://cars9.uchicago.edu/software/python/lmfit/contents.html

2.2. *COS Spectra*

The Barbara A. Mikulski Archive for Space Telescopes (MAST) archives yield 19 QSO targets observed by COS which lie within 500 kpc of our SALT galaxies. These targets vary widely in signal-to-noise from approximately 5 to 100 due to our choosing them based only on their proximity to galaxies with known rotation. The reduction procedure for these spectra follow those described by French & Wakker (2017) and Wakker et al. (2015). In short, spectra are processed with CALCOS v3.0 or higher and combined via the method of Wakker et al. (2015), which helps corrects the COS wavelength scale misalignments produced by CALCOS. Multiple exposures are combined via alignment with Galactic 21cm absorption spectra and summing total counts per pixel before converting to flux. The COS instrument is described in detail by Green et al. (2012).

3. HALO ROTATION MODEL

In order to better understand how QSO sightlines probe intervening velocity structure we have developed a simple halo gas rotation model. This model is seeded by an observed rotation curve (or whatever rotation curve-esque data suits ones fancy). This input curve is then interpolated and extended out to $2R_{vir}$ based on the average velocity of the outer 1/2 radius. Next, we project this interpolated rotation curve onto a plane oriented to a faux QSO sightline identically to the input galaxy-QSO pair orientation. By stacking multiple rotation-planes in the galaxy z-axis direction, we then create a simple cylindrical rotating halo model. Finally, each rotation-plane in the stack is projected onto the faux sightline. The result is a function representing the rotation velocity encountered by the sightline as a function of velocity (or distance) along it.

For each galaxy-QSO pair we created 2 rotation models: 1) a purely cylindrical halo extending $2R_{vir}$ in height and $3R_{vir}$ in radius, and 2) a cylindrical model extending $2R_{vir}$ in height and $3R_{vir}$ in radius with rotation velocities which smoothly decline based on a NFW profile fit (Navarro et al. 1996, 1997). Each model produces the velocity a co-rotating absorber would project onto the spectrum as a function of velocity along the sightline. We then collapse this into a simple range of possible observed velocities by summing the x- and y-components along the allowed range.

4. SALT GALAXIES

In this section we summarize each galaxy-QSO system observed by SALT. We calculate impact parameters to QSOs and galaxy-absorber velocity separations ($\Delta v = V_{Ly\alpha} - V_{sys}$) based on our measured V_{sys} values. Both measured and previously published values for V_{sys} are given in Table 1 for reference.

4.1. *CGCG039-137*

Table 1. SALT Galaxy Observations

Galaxy	R.A.	Dec.	Measured V_{sys} ($\mathrm{km\,s^{-1}}$)	Published V_{sys} ($\mathrm{km\,s^{-1}}$)	Type	Grating	V_{rot} ($\mathrm{km\,s^{-1}}$)	$V_{rot}/\sin(i)$ ($\mathrm{km\,s^{-1}}$)	Obs. Date	T_{exp} (ks)
(1)	(2)	(3)	(4)	(5)	(6)	(7)	(8)	(9)	(10)	(11)
CGCG039-137	11 21 27.0	+03 26 41.7	6918 ± 24	6902 ± 52[a]	Scd	PG2300	132 ± 16	139 ± 26	05 11 2016	700
ESO343-G014	21 37 45.2	−38 29 33.2	9139 ± 32	9162 ± 45[b]	S	PG2300	203 ± 32	203 ± 32	05 16 2016	1000
IC5325	23 28 43.4	−41 20 00.5	1512 ± 8	1503 ± 7[c]	SAB(rs)bc	PG2300	53 ± 5	125 ± 39	05 17 2016	600
MCG-03-58-009	22 53 40.9	−17 28 44.0	9015 ± 19	9030 ± 10[d]	Sc	PG2300	150 ± 12	171 ± 23	05 16 2016	1200
NGC1566	04 20 00.4	−54 56 16.1	1502 ± 15	1504 ± 2[e]	SAB(rs)bc	PG2300	64 ± 8	195 ± 47	10 18 2016	400
NGC3513	11 03 46.1	−23 14 43.8	1204 ± 12	1194 ± 7[f]	SB(s)c	PG2300	11 ± 10	22 ± 24	05 26 2016	600
NGC3633	11 20 26.2	+03 35 08.2	2587 ± 7	2600 ± 2[g]	SAa	PG2300	149 ± 6	157 ± 9	05 11 2016	1200
NGC4536	12 34 27.1	+02 11 17.3	1867 ± 33	1808 ± 1[h]	SAB(rc)bc	PG2300	129 ± 9	148 ± 41	05 11 2016	1300
NGC4939	13 04 14.4	−10 20 22.6	3093 ± 33	3110 ± 4[i]	SA(s)bc	PG2300	204 ± 25	275 ± 66	05 14 2016	500
NGC5364	13 56 12.0	+05 00 52.1	1238 ± 17	1241 ± 4[j]	SA(rs)bc pec	PG2300	130 ± 13	155 ± 22	05 11 2016	700
NGC5786	14 58 56.3	−42 00 48.1	2975 ± 22	2998 ± 5[k]	SAB(s)bc	PG2300	156 ± 10	172 ± 25	05 11 2016	250
UGC09760	15 12 02.4	+01 41 55.5	2094 ± 16	2023 ± 2[l]	Sd	PG2300	46 ± 10	46 ± 16	05 11 2016	500

NOTE—SALT targeted galaxies. Columns are as follows: 1) the galaxy name, 2), 3) R.A., Dec. in J2000, 4) galaxy systemic velocity, 5) morphological type (RC3), 6) RSS grating used, 7) approaching side velocity, 8) receding side velocity, 9) observation date, and 10) exposure time

[a] Abazajian et al. (2005)

[b] Jones et al. (2009)

[c] Corwin et al. (1994)

[d] Mathewson & Ford (1996)

[e] Koribalski et al. (2004)

[f] Corwin et al. (1994)

[g] Lu et al. (1993)

[h] Grogin et al. (1998)

[i] Koribalski et al. (2004)

[j] Corwin et al. (1994)

[k] di Nella et al. (1996)

[l] Giovanelli et al. (1997)

References—Giovanelli et al. (1997)

CGCG039-137 is an isolated Scd type galaxy with a measured systemic velocity of 6918 ± 24 $\mathrm{km\,s^{-1}}$ and inclination of 63°. The QSO RX_J1121.2+0326 is located nearby at an impact parameter of 99 kpc and azimuth angle of 71° on the receding side. The data for RX_J1121.2+0326 has low signal-to-noise (~ 4.2), but we are able to detect Lyα at 6975 $\mathrm{km\,s^{-1}}$, which, at $\Delta v = 57$ $\mathrm{km\,s^{-1}}$, lies well within the range of projected velocities consistent with co-rotation (cylindrical model = [-36, 137], NFW = [-37, 164] $\mathrm{km\,s^{-1}}$).

4.2. *ESO343-G014*

ESO343-G014 is an edge on spiral galaxy with a measured systemic velocity of 9139 ± 32 $\mathrm{km\,s^{-1}}$. It has a smaller neighboring galaxy, 2MASXJ21372816-3824412, located north of it's major axis at a projected distance of 216 kpc and velocity of 9129 $\mathrm{km\,s^{-1}}$. The nearest sightline is towards RBS1768 at an impact parameter of 466 kpc and 74° azimuth angle on the approaching side. We detect 3 blended Lyα absorption components toward RBS1768 at $V_{Ly\alpha} = 9308, 9360, 9434$ $\mathrm{km\,s^{-1}}$($\Delta v = 169, 221, 295$ $\mathrm{km\,s^{-1}}$). This system is highly blended and contaminated with galactic S I, and therefore their widths are not reliable. All of these are anti-aligned with the rotation of ESO343-G014 relative to the models (cylindrical = [-203, 10], NFW = [-122, 31] $\mathrm{km\,s^{-1}}$). Unfortunately the presence of 2MASXJ21372816-3824412 makes it difficult to attribute this gas solely to ESO343-G014. Additionally, this gas could be attributed to either the approaching or receding side of the disk due to the large impact parameter and high azimuth angle of the sightline.

Table 2. Summary of QSO Sample

Target	Galaxy	R.A.	Dec.	z	Program	T_{exp} (ks)
(1)	(2)	(3)	(4)	(5)	(6)	(7)
1H0419-577	NGC1566	04 26 00.7	-57 12 02.0	0.10400	11686	20429
2E1530+1511	NGC5951	15 33 14.3	+15 01 03.0	0.09000	14071	9348
3C232	NGC3067	09 58 20.9	+32 24 02.0	0.5306 0	8596	44662
3C273.0	NGC4536	12 29 06.7	+02 03 09.0	0.15834	12038	4002
CSO295	NGC3432	10 52 05.6	+36 40 40.0	0.60900	14772	1088
CSO1208	NGC3726	11 40 47.9	+46 22 05.0	0.11500	14729	3052
FBQSJ0908+3246	NGC2770	09 08 38.8	+32 46 20.0	0.25989	14240	7430
H1101-232	NGC3513	11 03 37.7	-23 29 31.0	0.18600	12025	13341
HE0429-5343	NGC1566	04 30 40.0	-53 36 56.0	0.04001	12275	2067
HE0435-5304	NGC1566	04 36 50.9	-52 58 47.0	0.42616	11520	8372
HE0439-5254	NGC1566	04 40 12.0	-52 48 18.0	1.05300	11520	8402
HE1228+0131	NGC4536	12 30 50.0	+01 15 23.0	0.11700	11686	11036
MRC2251-178	MCG-03-58-009	22 54 05.9	-17 34 55.0	0.06609	12029	5515
MRK335	NGC7817	00 06 19.5	+20 12 11.0	0.02578	11524	5122
MRK771	NGC4529	12 32 03.6	+20 09 30.0	0.06301	12569	1868
MRK876	NGC6140	16 13 57.2	+65 43 11.0	0.12900	11524	12579
MS1047.3+3518	NGC3432	10 50 10.9	+35 02 02.0	0.04125	8316	8301
PG0804+761	UGC04238	08 10 58.7	+76 02 43.0	0.10200	11686	5510
PG1259+593	UGC08146	13 01 12.9	+59 02 07.0	0.4778 0	11541	9200
PG1302-102	NGC4939	13 05 33.0	-10 33 19.0	0.27840	12038	5979
QSO1500-4140	NGC5786	15 03 34.0	-41 52 23.0	0.33500	11659	9258
RBS567	NGC1566	04 39 38.7	-53 11 31.0	0.24300	11520	8176
RBS1503	NGC5907	15 29 07.5	+56 16 07.0	0.09900	12276	1964
RBS1768	ESO343-G014	21 38 49.9	-38 28 40.0	0.18299	12936	6962
RBS2000	IC5325	23 24 44.7	-40 40 49.0	0.17359	13448	5046
RX_J1002.9+3240	NGC3067	10 02 54.5	+32 40 39.0	0.83000	12603	7713
RX_J1017.5+4702	NGC3198	10 17 31.0	+47 02 25.0	0.33544	13314	8655
RX_J1054.2+3511	NGC3432	10 54 16.2	+35 11 24.0	0.20300	14772	533
RX_J1117.6+5301	UGC06446	11 17 40.5	+53 01 51.0	0.15871	14240	4943
RX_J1121.2+0326	CGCG039-137	11 21 14.0	+03 25 47.0	0.15200	12248	2695
RX_J1121.2+0326	NGC3633	11 21 14.0	+03 25 47.0	0.15200	12248	2695
RX_J1142.7+4625	NGC3726	11 42 41.2	+46 24 36.0	0.11500	14772	2368
RX_J1236.0+2641	NGC4565	12 36 04.0	+26 41 36.0	0.20920	12248	4235
SBS1116+523	UGC06399	11 19 47.9	+52 05 53.0	0.35568	14240	4949
SBS1503+570	NGC5907	15 04 55.6	+56 49 20.0	0.35894	12276	5163
SDSSJ091052.80+333008.0	NGC2770	09 10 52.8	+33 30 08.0	0.11631	14240	7442
SDSSJ091127.30+325337.0	NGC2770	09 11 27.3	+32 53 37.0	0.29038	14240	10028
SDSSJ095914.80+320357.0	NGC3067	09 59 14.8	+32 03 57.0	0.56462	12603	2273
SDSSJ101622.60+470643.0	NGC3198	10 16 22.6	+47 06 43.0	0.82222	11598	4906
SDSSJ104335.90+115129.0	NGC3351	10 43 35.9	+11 05 29.0	0.79400	14071	4736
SDSSJ112005.00+041323.0	NGC3633	11 20 05.0	+04 13 23.0	0.54689	12603	4708
SDSSJ112224.10+031802.0	NGC3633	11 22 24.1	+03 18 02.0	0.47528	12603	7588
SDSSJ112439.50+113117.0	NGC3666	11 24 39.4	+11 31 17.0	0.14300	14071	10427
SDSSJ112448.30+531818.0	UGC06446	11 24 48.3	+53 18 19.0	0.53151	14240	7920
SDSSJ112632.90+120437.0	NGC3666	11 26 32.9	+12 04 37.0	0.97700	13314	8289
SDSSJ112756.70+115427.0	NGC3666	11 27 56.8	+11 54 27.0	0.50900	14145	5146
SDSSJ135726.27+043541.4	NGC5364	13 57 26.3	+04 35 41.0	1.23453	12264	14148
SDSSJ151237.15+012846.0	UGC09760	15 12 37.2	+01 28 46.0	0.26625	12603	7590
SDSSJ152053.59+571122.1	NGC5907	15 20 53.7	+57 11 23.0	0.02952	13654	3753
TON1009	NGC2770	09 09 06.2	+32 36 30.0	0.81028	12603	4740
TON1015	NGC2770	09 10 37.0	+33 29 24.0	0.35400	14240	4774

NOTE—Summary of COS targets in this sample.

4.3. *IC5325*

IC5325 is a face-on SAB(rs)bc type galaxy with a measured systemic velocity of 1512 ± 8 km s^{-1}. It's inclination is just high enough ($i = 25°$) to obtain a reasonable rotation curve. The closest neighboring galaxy is ESO347-G020 to the Southeast at 306 kpc and $V_{sys} = 1745$ km s^{-1}. Three other much smaller galaxies are also located ~ 450 kpc to the Southwest. We detect Lyα absorption at 1598 km s^{-1}($\Delta v = 86$ km s^{-1}) in the spectrum towards RBS2000 at an impact parameter of 314 kpc and azimuth angle of 64° on the approaching side. While this velocity is anti-aligned with the rotation the disk gas, the low inclination angle of IC5325 leads to a highly uncertain position angle. Without additional observations, we cannot say for certain if the location of RBS2000 actually lies on the approaching or receding side. This position angle uncertainty also means our SALT rotation curve is a lower limit on the true rotation velocity of IC5325.

4.4. *MCG-03-58-009*

MCG-03-58-009 is a massive and very isolated Sc type galaxy at a measured systemic velocity of 9015 ± 19 km s^{-1} and inclination angle of 49°. The QSO MRC2251-178 is located 355 kpc away at an azimuth angle of 71° on the receding side. We detect a weak Lyα absorber at $V_{Ly\alpha} = 9029$ km s^{-1}($\Delta v = 14$ km s^{-1}) towards MRC2251-178. This absorber velocity falls well within the expected range for co-rotation relative to our models (cylindrical = [-26, 137], NFW = [-42, 83] km s^{-1}). Although this absorber matches the velocity expected for co-rotation, the velocity difference ($\Delta v = 14$ km s^{-1}) is also within the systemic velocity uncertainty for MCG-03-58-009. The relative weakness of this absorber (EW = 62 ± 4 mÅ) is somewhat unusual given it's proximity (just outside of 1 R_{vir}) to a massive galaxy. If this is representative of an isolated system such as MCG-03-58-009, then we should expect the halo rotational velocity to approach systemic by 1 R_{vir}.

4.5. *NGC1566*

NGC1566 is a SAB(rs)bc type galaxy with measured systemic velocity of 1502 ± 15 km s^{-1} and inclination angle of 46°. There are several other large galaxies at $\rho \gtrsim 200$ kpc from NGC1566 (e.g., NGC1549, NGC1596, and NGC1581). The closest QSO sightline is toward HE0429-5343, northeast of NGC1566 at $\rho = 256$ kpc and 60° azimuth angle. We detect Lyα absorption toward HE0429-5343 at $V_{Ly\alpha} = 1167, 1358$ km s^{-1}($\Delta v = -335, -144$ km s^{-1}). Both of these absorbers have the correct velocity *sign*, but we would expect a smaller velocity for co-rotation based on our model results (cylindrical = [-53, -2], NFW = [-22, 17] km s^{-1}). Unfortunately NGC1617 is slightly closer to this sightline than NGC1566, at $\rho = 233$ kpc and $V_{sys} = 1063$ km s^{-1}, so it is not possible to confidently attribute these absorbers to NGC1566.

A more distant QSO sightline toward 1H0419-577 is located to the south at 303 kpc and just east of the receding side of the major axis at an azimuth angle of 10°. We detect Lyα at $V_{Ly\alpha} = 1123, 1188, 1264$ km s^{-1}($\Delta v = -379, -314, -238$ km s^{-1}), all of which are the wrong sign for co-rotation relative to our models (cylindrical = [48, 76], NFW = [-2, 31] km s^{-1}). This sightline is *also* actually closer to a small group of galaxies including NGC1549, NGC1546 and NGC1536, all with systemic velocities near ~ 1200 km s^{-1}. Additionally, this absorber system contains C III, C IV, Si II, Si III, Si IV lines. These lines likely are associated with this group rather than with NGC1566.

4.6. *NGC3513*

NGC3513 a mostly face-on SB(rs)c galaxy with measured systemic velocity $V_{sys} = 1204 \pm 12$ km s^{-1}. It has a companion galaxy in NGC3511 at an impact parameter of $\rho = 44$ kpc and $v_{sys} = 1109$ km s^{-1} (NGC3513 diameter $D = 22.1$ kpc, NGC3511 diameter $D = 28.1$ kpc). The background QSO H1101-232 is located directly south of the pair at 60 kpc and azimuth angle of 67° on the receding side. We detect Lyα at 1182 km s^{-1} toward H1101-232 ($\Delta v = -22$ km s^{-1}). NGC3513 appears to be rotating slowly, with a maximal inclination-corrected rotation velocity of $V_{rot}/\sin(i) = 22 \pm 24$ km s^{-1}. The $\Delta v = -22$ km s^{-1} for this absorber matches well with the magnitude of this rotation, but is opposite in sign for co-rotation on the sky and just outside our predicted model velocity range (cylindrical = [-19, 27], NFW = [-19, 28] km s^{-1}). Given that NGC3511 is so close, this absorber's velocity is probably subject to a complex velocity field influenced by both NGC3511 and NGC3513. This absorber system also contains C IV, N V, Si II, Si III, and Si IV lines.

4.7. *NGC3633*

NGC3633 is an isolated, edge-on SAa type galaxy with a measured systemic velocity of $V_{sys} = 2587 \pm 7$ km s^{-1}. Several locations along the disk of NGC3633 show two velocities for emission. We have combined these into a single velocity measurement via a weighted average.

The background QSO RX_J1121.2+0326 is located to the southeast at $\rho = 184$ kpc and 58° azimuth. We detect a Lyα absorber toward RX_J1121.2+0326 at $V_{Ly\alpha} = 2605$ km s^{-1} ($\Delta v = 18$ km s^{-1}) on the approaching side of NGC3633. While close to V_{sys}, this absorber velocity is just outside our predicted model velocities (cylindrical = [-153, -14], NFW = [-77, 10] km s^{-1}).

4.8. *NGC4536*

NGC4536 is a SAB(rs)bc type galaxy located in the Virgo Cluster at a measured systemic velocity of $V_{sys} = 1867 \pm 33$ km s^{-1}. The data on the receding side of

NGC4536 is quite messy, and may include contamination from background sources. Hence, our measured systemic velocity, and thus rotation velocity of 139 ± 37 km s^{-1}, have relatively high uncertainty. Other published redshift values available from NED and rotation velocities from the HyperLEDA database are broadly consistent with our values, albeit biased slightly lower and higher in velocity, respectively.

There are 2 sightlines to the southwest of NGC4536, both on the receding side of the galaxy. HE1228+0131 at ρ = 338 kpc and 86° azimuth has 5 Lyα lines: $V_{Ly\alpha}$ = 1495, 1571, 1686, 1721, 1854 km s^{-1} (Δv = −372, −296, −181, −146, −13 km s^{-1}). None of these are of the correct orientation for co-rotation relative to our model predictions (cylindrical = [18, 51], NFW = [2, 32] km s^{-1}), and all are more likely to be associated with other nearby galaxies, such as NGC4517A, which is slightly closer to these absorbers in impact parameter and velocity than is NGC4536. At $V_{Ly\alpha}$ = 1686 km s^{-1} we also detect C II, C IV, Si II, Si III, and Si IV, and at $V_{Ly\alpha}$ = 1721 km s^{-1} we detect Lyman series from $Ly\alpha$ to $Ly\theta$ as well as C II, C III, C IV, Si II, Si III, and Si IV.

The second nearby sightline is toward 3C273 at ρ = 344 kpc and 46° azimuth angle, and shows 3 Lyα lines at $V_{Ly\alpha}$ = 1580, 2156, 2267 km s^{-1} (Δv = −287, 289, 400 km s^{-1}). Two of these are correctly oriented for co-rotation relative to our model predictions (cylindrical = [87, 121], NFW = [5, 41] km s^{-1}), but are too high in velocity to make this scenario probable. Overall, given the number of nearby galaxies and their locations, we would expect these absorbers to trace the overall velocity field instead of the halo rotation of any particular galaxy.

4.9. *NGC4939*

NGC4939 is a large, fast rotating (V_{rot} = 275 ± 49 km s^{-1}) SA(s)bc type galaxy with measured systemic velocity V_{sys} = 3093 ± 33 km s^{-1}. The background QSO PG1302-102 is located at ρ = 254 kpc and 61° azimuth angle towards the southeast. We detect a Lyα absorber at $V_{Ly\alpha}$ = 3448 km s^{-1} (Δv = 355km s^{-1}) towards PG1302-102. This absorber is located on the approaching side of this galaxy, so we can easily rule out co-rotation in this case. NGC4939 does not have any close neighbors, so represents strong case against co-rotation for gas near or past 1 R_{vir}.

4.10. *NGC5364*

NGC5364 is a SA(rs)bc pec type galaxy at a measured systemic velocity of V_{sys} = 1238 ± 17 km s^{-1}. It is located in a group environment with 5 other large, nearby galaxies. The background QSO SDSSJ135726.27+043541.4 is located at ρ = 165 kpc and 84° azimuth angle on the receding side of NGC5364. We detect Lyα at $V_{Ly\alpha}$ = 967, 1124 km s^{-1} (Δv = −271, −114 km s^{-1}) toward SDSSJ135726.27+043541.4. These absorbers have the opposite sign for co-rotation relative to our model predictions (cylindrical = [-26, 108], NFW = [-30, 68] km s^{-1}). However, because of the orientation of NGC5364 on the sky with respect to this sightline, these absorbers lie extremely close to the inflection point were projected rotation velocities flip to approaching instead of receding. For example, shifting the location of SDSSJ135726.27+043541.4 east by a tenth of a degree (∼ 20 kpc) is sufficient to put these absorbers on the approaching side of NGC5364. Hence, both of these absorbers could be co-rotating with NGC5364 given very reasonable assumptions on the shape of an extended disk. Nonetheless, the fact that this system lives in galaxy group environment likely dominates the surrounding velocity field.

4.11. *NGC5786*

NGC5786 is a large, strongly-barred spiral galaxy with measured systemic velocity V_{sys} = 2975 ± 22 km s^{-1}. The background QSO QSO1500-4140 is located directly East at ρ = 453 kpc and 1° azimuth angle on the receding side of NGC5786. We detect Lyα at $V_{Ly\alpha}$ = 3138 km s^{-1} (Δv = 163 km s^{-1}) toward QSO1500-4140, which is slightly above the model predicted velocity range (cylindrical =[106, 160], NFW = [19, 67] km s^{-1}). However, the two neighboring galaxies ESO327-G038 and ESO327-G039 are both located south of NGC5786 at ρ = 62, 296 kpc, respectively. These nearby galaxies, along with the large distance to the absorption (∼ 2.5R_{vir}), make it difficult to believe this as evidence of an NGC5786 extended disk.

4.12. *UGC09760*

UGC09760 is an edge-on, slow-rotating Sd galaxy with measured systemic velocity V_{sys} = 2094 ± 16 km s^{-1}. This systemic velocity deviates slightly from other published redshifts, such as the The Updated Zwicky Catalog value of V_{sys} = 2023 ± 2 (Falco et al. 1999). This is likely due to our method of imposing rotation symmetry and averaging the approaching and receding velocities to derive V_{sys}. If we do not sample the rotation curve far enough out, a systematic offset is not unreasonable. Indeed, we do not detect the rotation curve turnover or flattening point.

The background QSO SDSSJ151237.15+012846.0 is located to the southeast at ρ = 123kpc and 90° azimuth angle. We detect Lyα absorption at $V_{Ly\alpha}$ = 2029 km s^{-1} (Δv = −65 km s^{-1}) toward SDSSJ151237.15+012846.0. This velocity falls outside the model predictions for co-rotation (cylindrical = [-30, 30], NFW = [-30, 86] km s^{-1}), but unfortunately this sightlines lies almost exactly at an azimuth of 90°. Hence, the motion of this gas gas could easily be either co-rotating or counter-rotating depending on a minute change in the position angle assigned to UGC09760. This is especially true if we assume our measured V_{sys}

is erroneously high, and indeed closer to the values obtained by other observations.

It is worth noting that there are several small satellite galaxies nearby, including SDSSJ151208.16+013508.5, SDSSJ151121.63+013637.6, SDSSJ151241.38+013723.7 and UGC09746 (impact parameters of 53, 88, 82, 230 kpc respectively). All of these galaxies lie slightly blueward of UGC09760, and thus *farther* away in velocity from the Lyα absorber at 2029 km s^{-1}.

5. ANCILLARY DATA

To increase our sample size we have also searched the literature for galaxies with published rotation curves and orientations. Unfortunately, while the rotation velocity is available for thousands of galaxies, only a handful also include the *orientation* of the rotation on the sky. Of these, we were able to find 18 additional galaxies which have a systemic velocity greater than ~ 500 km s^{-1}, and are near to a COS or STIS sightline with available data.

5.1. *NGC3198*

NGC3198 is a SB(rs)c type galaxy at $V_{sys} = 661 \pm 3$ km s^{-1}. It is a well studied galaxy, and is included the detailed THINGS rotation curve study of de Blok et al. (2008). We extracted the raw rotation curve derived by de Blok et al. (2008) using the plot digitization software WebPlotDigitizer[2]. NGC3198 has an even and flat rotation curve, with an average velocity of $v_{rot} = 152$ km s^{-1}. The background QSO RX_1017.5+4702 is located northeast at $\rho = 370$ kpc and 55° azimuth angle on the approaching side of NGC3198. We detect Lyα toward RX_1017.5+4702 at $V_{Ly\alpha} = 629$km s^{-1}($\Delta v = -32$ km s^{-1}), which can nicely be described by a co-rotating disk based on our model predicted velocity range (cylindrical = [-153, -21], NFW = [-91, 6] km s^{-1}). We note that the small dwarf galaxy SDSSJ101848.77+452137.0 is located 65 kpc away from NGC3198 toward the southwest.

SDSSJ101622.60+470643.0 is also located in the same direction but at a more distant 401 kpc away (**NOT IDENTIFIED**).

5.2. *NGC3351*

NGC3351 is a mostly face-on ($i = 29°$) SB(r)b type galaxy at $V_{sys} = 778 \pm 4$ km s^{-1}. It is located ~ 200 kpc southwest of the core of the Leo I group. We take the rotation curve and orientation produced by Dicaire et al. (2008). While we expect any extended disk rotation to be quickly disrupted due to the complex Leo I environment, this galaxy also has the closest sightline of our sample with SDSSJ104335.90+115129.0 at $\rho = 31$ kpc and 13° azimuth on the northwest, approaching side. We detect Lyα at $V_{Ly\alpha} = 717, 882, 1030$ km s^{-1}($\Delta v = -61, 104, 252$ km s^{-1}) toward this sightline. The lowest velocity absorber agrees nicely with both models for co-rotation, while the other two are above our model predictions (cylindrical = [-99, 12], NFW = [-68, 20] km s^{-1}). We also detect multiple metal ions associated with $V_{Ly\alpha} = 717$ km s^{-1} line, including C II, N I, N V, O I, Si II, Si III, Si IV, S II, and Fe II.

[2] WebPlotDigitizer; http://arohatgi.info/WebPlotDigitizer

5.3. *NGC5907*

NGC5907 is a large, edge-on SA(s)c type galaxy at $V_{sys} = 667$ km s^{-1}. We have taken the rotation curve and orientation information from Yim et al. (2014). The background QSO SBS1503+570 is located northwest at $\rho = 413$ kpc and 47° azimuth angle on the receding side of NGC5907. We detect *Ly*α at $V_{Ly\alpha} = 708$ km s^{-1} ($\Delta v = 41$ km s^{-1}), which falls within the model predictions for co-rotation (cylindrical = [31, 228], NFW = [-24, 101] km s^{-1}). Unfortunately there are several other nearby galaxies, the largest of which being NGC5866 ($D_{NGC5866} = 20.8$ and $\rho_{NGC5866} = 208$ kpc versus $D_{NGC5907} = 50.6$ and $\rho_{NGC5907} = 413$ kpc). Hence, it is difficult to assign this absorber to NGC5907 alone.

5.4. *NGC4565*

NGC4565 is an edge-on ($i = 75°$ SA(s)b type galaxy at a heliocentric velocity of 1230 km s^{-1}, for which we have taken the rotation curve and orientation from Sofue (1996). The sightline toward RX_J1236.0+2641, at 147 kpc and 41° azimuth angle on receding side, contains Lyα absorbers at velocities of 1009 and 1166 km s^{-1}($\Delta v = -221, -64$ km s^{-1}). Both are consistent with counter-rotating gas, although the line at 1166 km s^{-1}is close to the allowed range of [-29, 146] km s^{-1} for co-rotation. However, the presence of several satellite galaxies surely disrupts any possible extended disk rotation that would otherwise be detectable via sightline absorption.

5.5. *UGC06446*

UGC06446 is an Sd galaxy located at $V_{sys} = 645$ km s^{-1} on the far northwest edge of the Ursa Major cluster of galaxies. We take the rotation curve and orientation information from (Verheijen & Sancisi 2001; Swaters et al. 2009). We detect Lyα absorption toward two nearby QSO's, SDSSJ112448.30+531818.0 at 143 kpc and 22° azimuth (Lyα at 664 and 1019 km s^{-1}) and RX_J1117.6+5301 at 417 kpc and 52° azimuth (Lyα at 685 km s^{-1}), are both located toward the southwest, receding side of UGC06446. The absorbers residing at 664 km s^{-1} and 685 km s^{-1}both agree well with the expected velocities for co-rotating gas ([-15, 61], [25, 35]). The 1019 km s^{-1}absorber toward SDSSJ112448.30+531818.0 is most likely associated with NGC3718, which is much closer in velocity ($V_{sys} = 993$ km s^{-1}). Interestingly, we note that the more distant absorber toward RX_J1117.6+5301 has

a larger Δv value (Δv = 40 km s^{-1}compared to 19 km s^{-1}). If both absorbers were strictly following the expected NFW rotation curve, we would expect the opposite, with the more distant absorber velocity approaching V_{sys}.

5.6. *UGC06399*

UGC06399 is an edge-on Sm type galaxy located at V_{sys} = 791 km s^{-1} on the far west edge of the Ursa Major cluster of galaxies. Again, we take the rotation curve and orientation information from (Verheijen & Sancisi 2001; Swaters et al. 2009). As noted by Verheijen & Sancisi (2001), this is the most isolated galaxy in the Ursa Major cluster. Unfortunately, the closest QSO is SBS1116+523, at 471 kpc away on the northwest, approaching side. Although we detect Lyα absorption at 731 km s^{-1}, this impact parameter is beyond our model radius of $3R_{vir}$. Nonetheless, the velocity of this absorber agrees well with the expected velocity range if we extend a static or NFW rotating disk out to $4R_{vir}$.

5.7. *NGC3726*

The third galaxy from the Ursa Major galaxy cluster we're including is NGC3726, a SAB(r)c type galaxy at V_{sys} = 866 km s^{-1}on the southwestern edge of the cluster (Verheijen & Sancisi 2001). Two QSO's, CSO1208 and RX_J1142.7+4625, are located at 369 and 440 kpc, respectively, southeast of NGC3726. They lie very close to and on apposing sides of the minor axis, such that CSO1208 samples the receding side and RX_J1142.7+4625 the approaching. Unfortunately, both are also closer to a small group of dwarf galaxies, including NGC3782 and MCG+08-21-092, $\sim$ 100 km s^{-1} blueward of NGC3726. We detect Lyα at 731 and 874 km s^{-1} toward CSO1208. The 731 km s^{-1}line is most likely associated with the dwarf group, although the 874 km s^{-1} line falls within the expected range ([-28, 21]) for co-rotating gas.

CSO1208 at 369kpc, 87 az (Lya at 731, 874kms)
RX_J1142.7+4625 (PGC139665) at 440, 86 az (G130M but not in reduce) close to CSO1208

Both sightlines closer to some other little galaxies. NGC3877 nearby, has rot curve

5.8. *NGC3067*

The galaxy-QSO pair NGC3067-3C232 is a particularly well studied system. They are separated by only 11 kpc (74° azimuth angle on NW side) and a LLS of N_{HI} = 110^{20} cm^{-2} is detected toward 3C232 at 1421 km s^{-1}(V_{sys} = 1476 km s^{-1}), which has been postulated as a high velocity cloud (HVC) orbiting NGC3067 (Carilli et al. 1989; Keeney et al. 2005). We obtained the rotation curve for NGC3067 from Rubin et al. (1982) and the orientation from Carilli et al. (1989). While H I measurements of this LLS fit a single component, we have fit 3 separate components at 1408, 1510, and 1641 km s^{-1} to match the associated metal lines (namely, C IV, Si II, Si III, Si IV, Mg II, Fe II, and N I all show at least 2 separate components). This splitting has been analyzed in detail most recently by Keeney et al. (2005) and Stocke et al. (2010), who find similar but slightly lower cz for all three absorbers.

3C232 is located directly north of NGC3067, thus placing it on the receding side. Our NFW model predicts a co-rotating cloud to have a velocity within the range [-139, 26] km s^{-1}. Hence, the 1408 and 1510 km s^{-1}lines can be described as co-rotating (assuming reasonable velocity uncertainties), while the 1641 km s^{-1}line must be either a counter-rotating cloudlet or an outflow directed away from our line of sight.

SDSSJ095914.80+320357.0 at 128 kpc, 43 az (not ID'd, but probable line around 1500kms)
RX_J1002.9+3240 at 359 kpc, 33 az (not in reduce yet)

We have also included the 5 galaxy-QSO systems analyzed by Côté et al. (2005). We briefly summarize each of these systems here, and refer the reader to Côté et al. (2005) for a more complete discussion. **ALL? OF THESE GALAXIES WE PROJECT TO BE AT GREATER IMPACT PARAMETER THAN COTE DID. MOSTLY BASED ON BETTER RID DISTANCES THAN USED BY COTE**

5.9. *NGC6140*

NGC6140 is a small SB(s)cd_pec type galaxy located at V_{sys} = 910 km s^{-1} and 113 kpc from the sightline toward QSO MRK876. The approaching side is oriented toward the east, with MRK876 toward the northwest at an azimuth of 21° (although this is somewhat uncertain; the position angle for NGC6140 could be closer to 60° than our adopted value of 94° due to it being mostly face on, faint, and strongly barred). We detect Lyα absorption toward MRK876 at 939 km s^{-1}(Δv = 29 km s^{-1}). This value implies co-rotation, but is just below the range predicted by our models (35 - 102 km s^{-1}).

5.10. *NGC4529*

As an inclined, isolated galaxy with a QSO sightline located 159 kpc and only 23° off the major axis, NGC4529 represents an ideal test environment for this study. This sightline towards MRK771 contains a Lyα absorber at 2553 km s^{-1}. With V_{sys} = 2536 km s^{-1} and MRK771 located on the approaching side of NGC4529 (southwest side), this is a clearcut case of counter-rotating H I. As Côté et al. (2005) conclude, "there is simply no physical way to produce such a velocity with an extending co-rotating disk."

5.11. *UGC04238*

UGC04238 is an isolated and edge-on SBd type galaxy at $V_{sys} = 1544$ km s^{-1}. We take the rotation curve and orientation from Côté et al. (2005). Lyα are detected at 1143, 1526, and 1593 km s^{-1}toward PG0804+761, located directly south at 148 kpc and 59° azimuth on the receding side of UGC04238. Only the absorber at 1593 km s^{-1}, the lowest W of the three, falls within the expected velocity range for co-rotation.

The following are from Rhee & van Albada (1996):

5.12. *NGC2770*

NGC2770 is a large, edge-on Sc type galaxy at $V_{sys} = 1947$ km s^{-1}. It is mostly isolated except for two nearby small dwarfs MCG+06-20-036NED02 and GALEXASCJ090946.88+330840.4 (both 25 kpc away, on opposite sides of NGC2770). We take the rotation curve and orientation from Rhee & van Albada (1996). There are five nearby QSOs. Toward the south on the approaching side they are the following: FBQSJ0908+3246 at 204 kpc and 59° azimuth (Lyα at 1915, 1982 km s^{-1}), TON1009 at 267 kpc and 41° azimuth (**NEEDS TO BE IDENTIFIED**), and SDSSJ091127.30+325337.0 at 234 kpc and 30° azimuth (Lyα at 2063 km s^{-1}). Only the 1915 km s^{-1} line can reasonably be explained by co-rotation.

Toward the northeast on the receding side they are the following: TON1015 at 218 kpc and 61° azimuth (Lyα at 1833, 1985 km s^{-1}), and SDSSJ091052.80+333008.0 at 239 kpc and 66° azimuth (Lyα at 1824, 1975 km s^{-1}). Two of these lines, at 1985 km s^{-1} and 1975 km s^{-1} are consistent with co-rotation. Interestingly, these two QSO's appear to be sampling the same structures. The absorber pairs at 1833, 1824 km s^{-1} and 1985, 1975 km s^{-1} each have the equivalent EW and $N_{H\,i}$ within errors, and remarkably similar appearing line-structure. Adopting a distance of 28.6 Mpc to this cloud, we calculate a linear separation between TON1015 and SDSSJ091052.80+333008.0 of 28 kpc. Hence, there appears to be two distinct clouds of at least 28 kpc in physical extent sandwiched around the system velocity of NGC2770. **MORE?**

5.13. *NGC3432*

NGC3432 is an edge-on SB(s)m type galaxy at $V_{sys} = 616$ km s^{-1}. It is interacting with the nearby dwarf galaxy UGC05983 located 11 kpc away and at $V_{sys} = 765$ km s^{-1}. We take a rotation curve and orientation for NGC3432 from Rhee & van Albada (1996). The quasar CSO295 is located just 20 kpc away and just to the receding side of the minor axis. This is the second closest pair in our sample, after the 11 kpc separated NGC3067-3C232 system. We detect Lyα toward CSO295 at 600 and 662 km s^{-1}. Both of these lines fall well within our expected range for co-rotation ([-37, 134] km s^{-1} for an NFW halo). This would represent the lower-velocity cloud existing toward the near-edge of the halo and the higher velocity cloud lying very close to the plane of the stellar disk.

CSO295 at 20 kpc, 82 az (Lya 600, 662), [-37, 134]NFW
RX_J1054.2+3511 at 290 kpc, 57 az (Looks like a feature around 600 km s^{-1} but no ID?)
MS1047.3+3518 at 326 kpc, 26 az (low SN, not ID'd, possible feature?)
SDSSJ110349.70+371527.0 (low res only)

5.14. *NGC3666*

NGC3666 is a mostly isolated and edge-on SA(rs)c type galaxy at $V_{sys} = 1060$ km s^{-1}. We take a rotation curve and orientation from Rhee & van Albada (1996). The following three QSOs are located toward on the approaching, northeast side: SDSSJ112439.50+113117.0 at 58 kpc, SDSSJ112632.90+120437.0 at 279 kpc, and SDSSJ112756.70+115427.0 at 320 kpc. There are several dwarf galaxies $\sim$ 400 kpc away, but all are more distant than these three QSOs. We detect Lyα toward SDSSJ112439.50+113117.0 at 1047 and 1099 km s^{-1}($\Delta v = -13, 39$ km s^{-1}).

SDSSJ112439.50+113117.0 at 58 kpc - Borthakur target (Lya at 1047, 1099 km s^{-1}), [-87, 20], [-136, 20]NFW
SDSSJ112632.90+120437.0 at 279 kpc - Borthakur target (not in reduce yet)
SDSSJ112756.70+115427.0 at 320 kpc - (not in reduce yet)

NW side is receding

5.15. *NGC5951*

NGC5951 is a large, edge-on SBc type galaxy at $V_{sys} = 1780$ km s^{-1}. The pair of galaxies NGC5954 and NGC5953 are nearby ($\sim$ 100 kpc), but the sightline toward 2E1530+1511 is closer ($\rho = 55$ kpc straight east of NGC5951) and on the opposite side (85° azimuth). We take the rotation curve and orientation for NGC5951 from Rhee & van Albada (1996). Lyα appears toward 2E1530+1511 at 1795 and 1953 km s^{-1}($\Delta v = 15, 173$ km s^{-1}). The absorber at 1795 km s^{-1} aligns well with co-rotation, but the 1953 km s^{-1} absorber has a great velocity than V_{rot} for NGC5951. Given the V_{sys} for the nearby galaxies NGC5954 and NGC5953 are 1959 and 1965 km s^{-1}, this absorber is likely also linked with that system.

5.16. *NGC7817*

NGC7817 is an edge-on SAbc type galaxy at $V_{sys} = 2309$ km s^{-1}. We take a rotation curve and orientation from Rhee & van Albada (1996). The dwarf galaxy ESDOF538-02 is the closest neighbor, at 57 kpc to the

east. A sightline toward MRK335 is located 343 kpc toward the southeast, lying directly on the projected minor axis of NGC7817. Because of this our model predicts a narrow range of velocities for co-rotation ([-26, -24] km s^{-1}). Lyα absorbers are detected at 1954 and 2274 km s^{-1}, the latter of which falling a mere 9 km s^{-1} outside this predicted range. Within a very reasonable level of uncertainty this 2274 km s^{-1} absorber could easily be co-rotating with NGC7817. The absorption at 1954 km s^{-1} is likely not directly associated with NGC7817, given the large velocity difference.

5.17. *UGC08146*

UGC08146 is an isolated and edge-on Sd type galaxy at $V_{sys} = 670$ km s^{-1}. This galaxy (and the nearby QSO PG1259+593) are included in the Côté et al. (2005) sample also, but we have taken the rotation curve and orientation from Rhee & van Albada (1996). PG1259+593 is located 114 kpc northwest of UGC08146, at 50° azimuth on the receding side. While Côté et al. (2005) cite a single Lyα component at 679 km s^{-1}, we find two components, at 646 and 683 km s^{-1}, in the higher signal-to-noise COS data now available for PG1259+593. Both of these components are consistent with co-rotating gas, assuming reasonable uncertainty in V_{sys}, $V_{Ly\alpha}$, and V_{rot}.

Table 3. Halo Model Results and Lyα Absorption Properties

Galaxy	Target	ρ	Az.	V_{sys}	V_{rot}	$V_{Ly\alpha}$	$W_{Ly\alpha}$	Cyl. Model	NFW Model
		(kpc)	(Deg.)	(km s^{-1})	(km s^{-1})	(km s^{-1})	(mÅ)	(km s^{-1})	(km s^{-1})
(1)	(2)	(3)	(4)	(5)	(6)	(7)	(8)	(9)	(10)
CGCG039-137	RX_J1121.2+0326	99	71	6917.8	139	6975	678	[-36, 137]	[-37, 164]
CGCG039-137	SDSSJ112224.10+031802.0	491	24	6917.8	-139	6606	70	[-129, -115]	[-115, -99]
ESO343-G014	RBS1768	466	74	9138.9	205	9308	63	[-203, 10]	[-122, 31]
ESO343-G014	RBS1768	466	74	9138.9	205	9360	306	[-203, 10]	[-122, 31]
ESO343-G014	RBS1768	466	74	9138.9	205	9434	161	[-203, 10]	[-122, 31]
IC5325	RBS2000	314	64	1511.9	-125	1598	35	[-41, -20]	[-29, 1]
MCG-03-58-009	MRC2251-178	355	71	9014.9	171	9029	62	[-26, 137]	[-42, 83]
NGC1566	1H0419-577	303	10	1501.9	86	1075	249	[48, 76]	[-2, 31]
NGC1566	1H0419-577	303	10	1501.9	86	1123	269	[48, 76]	[-2, 31]
NGC1566	1H0419-577	303	10	1501.9	86	1188	240	[48, 76]	[-2, 31]
NGC1566	1H0419-577	303	10	1501.9	86	1264	91	[48, 76]	[-2, 31]
NGC1566	1H0419-577	303	10	1501.9	86	2020	9	[48, 76]	[-2, 31]
NGC1566	HE0429-5343	256	60	1501.9	-86	1167	79	[-53, -2]	[-22, 17]
NGC1566	HE0429-5343	256	60	1501.9	-86	1358	136	[-53, -2]	[-22, 17]
NGC1566	HE0435-5304	396	62	1501.9	-86	1512	220	[-44, -43]	[-16, -15]
NGC1566	HE0435-5304	396	62	1501.9	-86	1633	217	[-44, -43]	[-16, -15]
NGC1566	HE0435-5304	396	62	1501.9	-86	1690	204	[-44, -43]	[-16, -15]
NGC1566	RBS567	423	69	1501.9	-86	1664	517	[-46, -7]	[-22, 10]
NGC1566	HE0439-5254	459	65	1501.9	-86	1148	72	[-50, -22]	[-23, 1]
NGC1566	HE0439-5254	459	65	1501.9	-86	1649	501	[-50, -22]	[-23, 1]
NGC3513	H1101-232	60	67	1203.7	20	1182	635	[-19, 27]	[-19, 28]
NGC3633	SDSSJ112224.10+031802.0	413	50	2587.2	-157	-99	-99	[-158, -51]	[-64, 0]
NGC3633	SDSSJ112005.00+041323.0	468	78	2587.2	-157	2285	27	[-59, -55]	[-36, -28]
NGC3633	SDSSJ112005.00+041323.0	468	78	2587.2	-157	2578	116	[-59, -55]	[-36, -28]
NGC3633	RX_J1121.2+0326	184	58	2587.2	-157	2605	180	[-153, -14]	[-77, 10]
NGC4536	3C273.0	349	11	1866.9	139	1580	369	[87, 121]	[5, 41]
NGC4536	3C273.0	349	11	1866.9	139	2156	42	[87, 121]	[5, 41]
NGC4536	3C273.0	349	11	1866.9	139	2267	27	[87, 121]	[5, 41]
NGC4536	HE1228+0131	338	51	1866.9	139	1495	160	[18, 51]	[2, 32]
NGC4536	HE1228+0131	338	51	1866.9	139	1571	23	[18, 51]	[2, 32]
NGC4536	HE1228+0131	338	51	1866.9	139	1686	321	[18, 51]	[2, 32]
NGC4536	HE1228+0131	338	51	1866.9	139	1721	303	[18, 51]	[2, 32]
NGC4536	HE1228+0131	338	51	1866.9	139	1854	78	[18, 51]	[2, 32]
NGC4536	HE1228+0131	338	51	1866.9	139	2311	343	[18, 51]	[2, 32]
NGC4939	PG1302-102	254	61	3092.8	-275	3448	72	[-219, 14]	[-119, 36]

Table 3 continued

Table 3 *(continued)*

Galaxy	Target	ρ	Az.	V_{sys}	V_{rot}	$V_{Ly\alpha}$	$W_{Ly\alpha}$	Cyl. Model	NFW Model
		(kpc)	(Deg.)	(km s^{-1})	(km s^{-1})	(km s^{-1})	(mÅ)	(km s^{-1})	(km s^{-1})
(1)	(2)	(3)	(4)	(5)	(6)	(7)	(8)	(9)	(10)
NGC5364	SDSSJ135726.27+043541.4	165	84	1238	55	1124	83	[-26, 108]	[-30, 68]
NGC5364	SDSSJ135726.27+043541.4	165	84	1238	55	1296	92	[-26, 108]	[-30, 68]
NGC5786	QSO1500-4140	453	1	2974.6	172	3141	177	[106, 160]	[19, 67]
UGC09760	SDSSJ151237.15+012846.0	123	90	2093.7	-46	2051	496	[-30, 30]	[-30, 86]
NGC3198	RX_J1017.5+4702	370	55	660	152	629	71	[-153, -21]	[-91, 6]
NGC3198	SDSSJ101622.60+470643.0	401	61	660	152	-99	-99	[-154, -17]	[-89, 8]
NGC4565	RX_J1236.0+2641	147	41	1230	253	1009	365	[-2, 246]	[-30, 144]
NGC4565	RX_J1236.0+2641	147	41	1230	253	1166	305	[-2, 246]	[-30, 144]
UGC04238	PG0804+761	148	59	1544	91.6	1143	183	[-3, 86]	[-6, 94]
UGC04238	PG0804+761	148	59	1544	91.6	1526	62	[-3, 86]	[-6, 94]
UGC04238	PG0804+761	148	59	1544	91.6	1593	32	[-3, 86]	[-6, 94]
NGC3351	SDSSJ104335.90+115129.0	31	43	778	198	717	823	[-99, 12]	[-68, 20]
NGC3351	SDSSJ104335.90+115129.0	31	43	778	198	882	621	[-99, 12]	[-68, 20]
NGC3351	SDSSJ104335.90+115129.0	31	43	778	198	1030	391	[-99, 12]	[-68, 20]
NGC4529	MRK771	159	23	2536	106.4	2553	240	[-103, -40]	[-105, -35]
NGC6140	MRK876	113	21	910	138.11	939	379	[40, 101]	[35, 102]
NGC5907	SBS1503+570	413	47	667	227.4	708	301	[31, 228]	[-24, 101]
NGC5907	SDSSJ152053.59+571122.1	286	63	667	227.4	-99	-99	[-18, 228]	[-42, 114]
NGC5907	RBS1503	478	63	667	227.4	-99	-99	[-228, -9]	[-96, 33]
UGC06446	RX_J1117.6+5301	417	52	645	79.4	685	342	[35, 47]	[24, 35]
UGC06446	SDSSJ112448.30+531818.0	143	22	645	79.4	664	339	[-9, 65]	[-15, 61]
UGC06446	SDSSJ112448.30+531818.0	143	22	645	79.4	1019	71	[-9, 65]	[-15, 61]
UGC06399	SBS1116+523	471	13	791	88.2	731	259	[-91, -54]	[-80, -42]
NGC3726	CSO1208	369	88	866	167.2	731	470	[-27, 29]	[-28, 21]
NGC3726	CSO1208	369	88	866	167.2	874	506	[-27, 29]	[-28, 21]
NGC3726	RX_J1142.7+4625	440	86	866	167.2	818	375	[-34, -14]	[-30, -7]
NGC3067	3C232	11	74	1476	148.2	1408	2092	[-121, 25]	[-139, 26]
NGC3067	3C232	11	74	1476	148.2	1510	700	[-121, 25]	[-139, 26]
NGC3067	3C232	11	74	1476	148.2	1641	1635	[-121, 25]	[-139, 26]
NGC3067	SDSSJ095914.80+320357.0	128	43	1476	148.2	-99	-99	[11, 138]	[-12, 81]
NGC3067	RX_J1002.9+3240	359	33	1476	148.2	-99	-99	[115, 147]	[42, 65]
NGC2770	FBQSJ0908+3246	204	59	1947	150	1915	202	[-146, -4]	[-132, 6]
NGC2770	FBQSJ0908+3246	204	59	1947	150	1982	230	[-146, -4]	[-132, 6]
NGC2770	TON1009	267	41	1947	150	-99	-99	[-146, -39]	[-125, -20]
NGC2770	TON1015	218	61	1947	150	1833	244	[3, 146]	[-7, 130]
NGC2770	TON1015	218	61	1947	150	1985	80	[3, 146]	[-7, 130]
NGC2770	SDSSJ091052.80+333008.0	218	66	1947	150	1824	266	[6, 145]	[-4, 127]
NGC2770	SDSSJ091052.80+333008.0	239	66	1947	150	1975	68	[6, 145]	[-4, 127]
NGC2770	SDSSJ091127.30+325337.0	234	30	1947	150	2063	271	[-150, -43]	[-132, -25]
NGC3432	CSO295	20	82	616	122	600	568	[-37, 48]	[-37, 134]
NGC3432	CSO295	20	82	616	122	662	585	[-37, 48]	[-37, 134]
NGC3432	RX_J1054.2+3511	290	57	616	122	703	184	[0, 123]	[-9, 111]
NGC3432	MS1047.3+3518	326	26	616	122	-99	-99	[35, 124]	[19, 109]
NGC3666	SDSSJ112439.50+113117.0	58	83	1060	131.8	1047	345	[-87, 20]	[-136, 20]
NGC3666	SDSSJ112439.50+113117.0	58	83	1060	131.8	1099	272	[-87, 20]	[-136, 20]
NGC3666	SDSSJ112632.90+120437.0	279	65	1060	131.8	-99	-99	[-59, -29]	[-45, -18]
NGC3666	SDSSJ112756.70+115427.0	320	43	1060	131.8	-99	-99	[-127, -80]	[-100, -57]
NGC5951	2E1530+1511	55	85	1780	127.9	1795	507	[-31, 114]	[-32, 136]
NGC5951	2E1530+1511	55	85	1780	127.9	1953	137	[-31, 114]	[-32, 136]
NGC7817	MRK335	343	90	2309	180.4	1954	216	[-26, -24]	[-26, -24]
NGC7817	MRK335	343	90	2309	180.4	2274	150	[-26, -24]	[-26, -24]
UGC08146	PG1259+593	114	50	670	82.4	646	133	[-13, 82]	[-15, 91]

Table 3 continued

Table 3 *(continued)*

Galaxy	Target	ρ	Az.	V_{sys}	V_{rot}	$V_{Ly\alpha}$	$W_{Ly\alpha}$	Cyl. Model	NFW Model
		(kpc)	(Deg.)	(km s^{-1})	(km s^{-1})	(km s^{-1})	(mÅ)	(km s^{-1})	(km s^{-1})
(1)	(2)	(3)	(4)	(5)	(6)	(7)	(8)	(9)	(10)
UGC08146	PG1259+593	114	50	670	82.4	683	168	[-13, 82]	[-15, 91]

NOTE—Comments.

6. DISCUSSION

In this section we consider in aggregate our sample of Lyα absorbers, and the fraction consistent with co-rotation under various cuts and constraints.

To start we consider the fraction of absorbers which appear to be rotating in the same sense as the nearby galaxy. With no cuts of any kind, we find 46% of absorbers have velocities of the "correct" sign (versus 35% "incorrect") to be rotating in the same sense as the nearby galaxies. However, many of these absorbers have a velocity difference, Δv, larger than the inclination-corrected galaxy rotation velocity (V_{rot}). This results in a much smaller fraction of co-rotating absorbers when compared to our cylindrical and NFW profile models (28% and 29%, respectively), which will never output an absorber velocity higher than V_{rot}. In undertaking this study we are assuming that absorption within some velocity limit and impact parameter from a galaxy is likely associated with that galaxy. To start with we set these limits at $\Delta v_{max} = 400$ km s^{-1} and $\rho_{max} = 3R_{vir}$.

Let us now instead consider only absorbers with $\Delta v \leq V_{rot} \pm 10$ km s^{-1}, or absorbers with velocities differences no greater than the maximal galaxy rotation velocity ($\pm$ a 10 km s^{-1} buffer to account for velocity uncertainties). With this constraint the co-rotating fraction increases to 50%.[3] One additional constraining step we take is to only consider galaxies which have no neighbors within at least 20 kpc. The disruptions caused by near neighbors to both galaxy H I disks and halos has been well established observationally, so a 20 kpc minimum separation should at least remove the systems most likely to be disrupted. This constraint alone leads to a co-rotating fraction of 40%. Combining both constraints results in a 54% co-rotating fraction.

Next, we consider the effect of galaxy luminosity. We separate our sample about 0.5 L^*, while keeping our $\Delta v \leq V_{rot} \pm 10$ km s^{-1}constraint and relaxing the 20 kpc nearest-neighbor criteria in order to maximize the sample size. This results in 10 absorbers near $L \leq 0.5L^*$ galaxies and 34 around more luminous galaxies. The co-rotating fraction around luminous galaxies is then 32%, compared to 100% around $L \leq 0.5L^*$ galaxies. In fact, the co-rotating absorber fraction smoothly decreases as a function of L^*, as shown in Figure 1.

Finally, we consider the Doppler b-parameters of our absorber sample. Figure 3 shows the distribution of b-parameters for all Lyα absorbers with $V_{Ly\alpha} \leq V_{rot} \pm 10$ km s^{-1}. In the top panel we separate them into co-rotating and anti-rotating subsets, in the middle panel we do the same but only for $\rho \leq 1R_{vir}$, and on the bottom we separate based on absorbers near $L^* \leq 0.5$ and $L^* > 0.5$ galaxies. Interestingly, we find that *higher* b-parameter absorbers tend to be both co-rotating and found near $L^* \leq 0.5$ galaxies. The picture described by Stewart et al. (2011), however, **FIND MORE AND NEWER CITATIONS** describes a scenario where co-rotating gas is predominately the product of cold-mode accretion. Hotter, outflowing gas would likely carry angular momentum from the disk with it, but this would be quickly lost as the outflows expand into the halo and result in negligible observable rotation. In Figure 2 we show how the b-parameters vary as a function of Δv for co-rotating versus anti-rotating absorbers. We would expect the co-rotating sample to occupy a narrower Δv space based on their definition (Δv fitting within the velocity bounds given by our model), but the elevated b-parameters for these compared to the relatively flat distribution for anti-rotators is intriguing.

Lutz et al. (2018) find that galaxies with high H I mass compared to their stellar mass have higher halo angular momentum, which may be impeding their ability to efficiently form stars. While we do not have independent measures of H I and stellar mass for our galaxies, it may not be unreasonable to think that these high angular momentum galaxies reside toward the lower luminosity end of our sample.

7. SUMMARY

8. SIGHTLINES NEEDED

The following targets need to be added:
SBS1304+594
SDSSJ112632.90+120437.0
SDSSJ112756.70+115427.0
RX_J1054.2+3511 - check for feature around 600 km s^{-1}
MS1047.3+3518
RX_J1002.9+3240
SDSSJ152053.59+571122.1
SDSSJ104816.30+120735.0
SDSSJ104709.80+130454.0
SDSSJ104843.50+130605.0

[3] From here on we concentrate on the results using our NFW profile model. The cylindrical model results do not differ in a systematically interesting way.

Table 4. Results

Sub-sample	Co-rotating	Anti-rotating	Uncertain	Co-rotating $\rho \leq 1$	Anti-rotating $\rho \leq 1$	Co-rotating $\rho > 1$	Anti-rotating $\rho > 1$
Apparent Vel.	37	28	15	9	7	28	21
Cyl. Model	22	44	14	8	9	14	35
NFW Model	23	43	14	8	9	15	34
NFW w/ Constraint: $V_{Ly\alpha} \leq V_{rot}$	22	16	6	7	5	15	11
NFW w/ Constraint: Nearest $\rho \geq 20$ kpc	14	16	5	4	2	10	14
NFW w/ Both Constraints	13	9	2	3	1	10	8
NFW w/ V_{rot} Constraint: $[0 \leq L^* \leq 0.5]$	10	0	0	2	0	5	1
NFW w/ V_{rot} Constraint $[L^* > 0.5]$	12	16	6	3	9	5	11

Note—Comments.

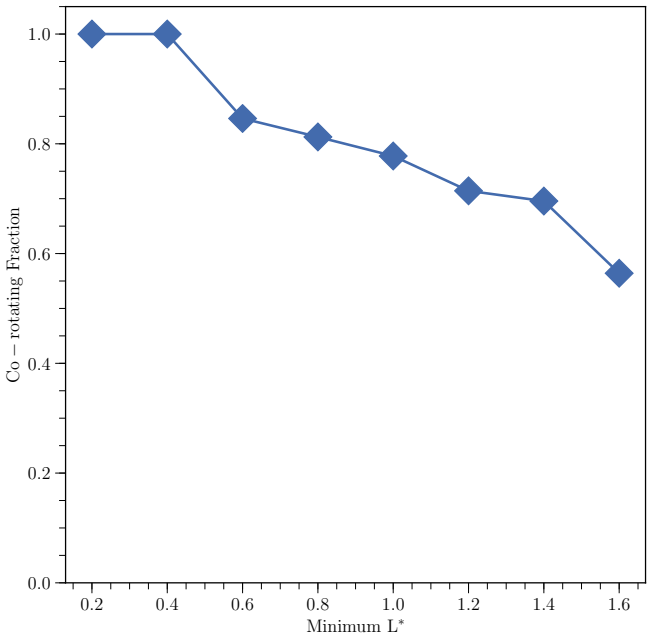

Figure 1. The fraction of co-rotating absorbers as a function of minimum L^*. All systems are included at L^*=1.6 (this bin includes galaxies brighter than $1.6L^*$ as well), then only galaxies with $L^* \leq 1.4$ are included at L^* =1.4, and so on.

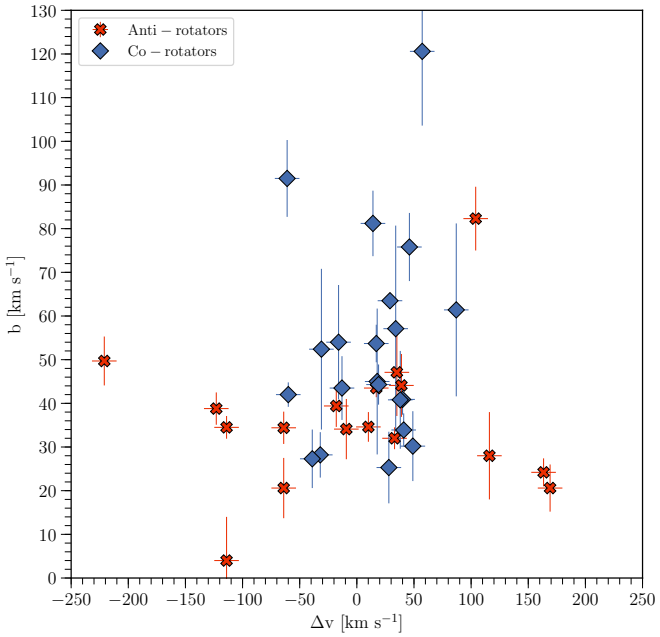

Figure 2. The Doppler b-parameters of each absorber as a function of Δv, split into co-rotating (blue diamonds) and anti-rotating (red crosses). The data point for the NGC3067-3C232 LLS ($b = 245.2 \pm 25.9$, $\Delta v = -68.0 \pm 11$ km s^{-1}) is not shown in order to highlight the majority distribution in greater detail.

SDSSJ105220.60+101751.0
SDSSJ104341.53+085558.2
SDSSJ101622.60+470643.0

D. M. F. thanks Claire Murray for useful insights on our halo model, and Julie Davis for invaluable SALT data reduction pointers. This research has made use of the NASA/IPAC Extragalactic Database (NED) which is operated by the Jet Propulsion Laboratory, California Institute of Technology, under contract with the National Aeronautics and Space Administration. Based on observations with the NASA/ESA *Hubble Space Telescope*, obtained at the Space Telescope Science Institute (STScI), which is operated by the Association of Universities for Research in Astronomy, Inc., under NASA contract NAS 5-26555. **SALT ACKNOWL-**

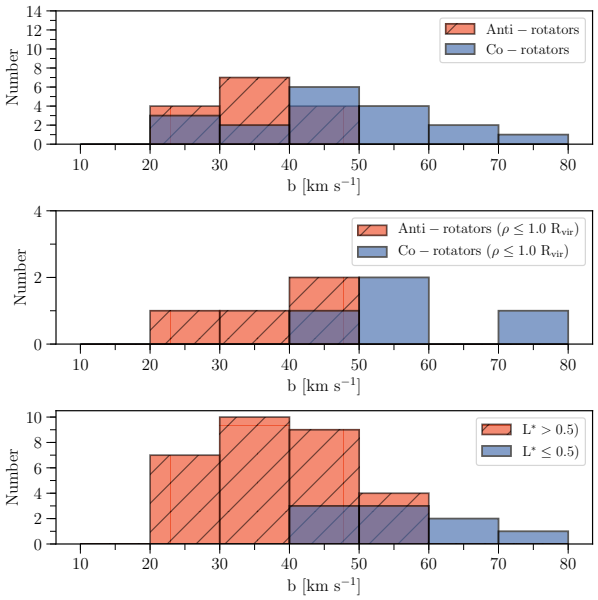

Figure 3. Histograms showing the distributions of Doppler b-parameters for all Lyα absorbers with $V_{Ly\alpha} \leq V_{rot} \pm 10$ km s^{-1}. In the top panel we separate them into co-rotating (blue) and anti-rotating (red-hatched) subsets, in the middle we do the same but only for $\rho \leq 1R_{vir}$, and on the bottom we separate based on absorbers near $L^* \leq 0.5$ (blue) and $L^* > 0.5$ (red-hatched) galaxies.

EDGEMENT. Spectra were retrieved from the Barbara A. Mikulski Archive for Space Telescopes (MAST) at STScI. Over the course of this study, D.M.F. and B.P.W. were supported by grant AST-1108913, awarded by the US National Science Foundation, and by NASA grants *HST*-AR-12842.01-A, *HST*-AR-13893.01-A, and *HST*-GO-14240 (STScI).

Facility: HST (COS), SALT (RSS)

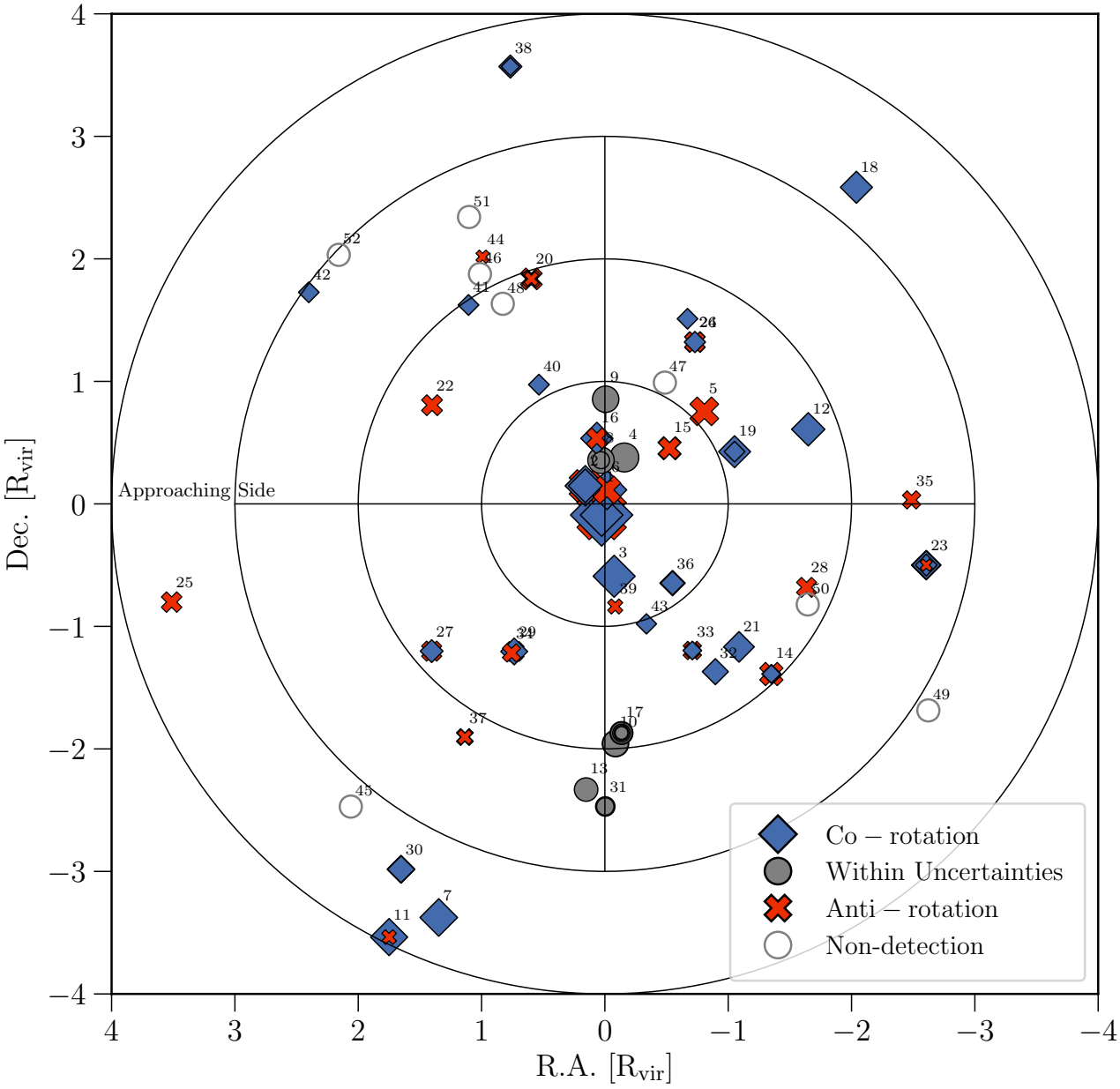

Figure 4. A map of the locations of each absorber normalized with respect to the galaxy virial radius. The color and style of each point indicates the line-of-sight velocity compared to that of the rotation of the nearby galaxy. Blue diamonds indicate co-rotation, red crosses indicate anti-rotation, and grey circles indicate cases where either is possible due to a combination of orientation and velocity uncertainties. The size of each point is scaled to reflect the EW of the absorber. Concentric rings indicate distances of 1, 2, 3 and 4 R_{vir}. All galaxies are rotated to PA = 90 or 270, such that their major axis' are horizontal and their approaching side is on the left as indicated.

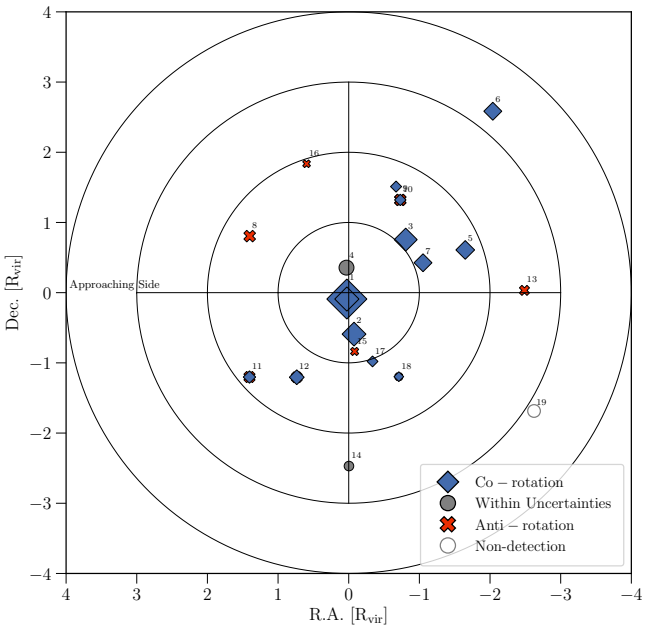

Figure 5. A map of the locations of each absorber normalized with respect to the galaxy virial radius. The color and style of each point indicates the NFW rotation model results for each absorber with $V_{Ly\alpha} \leq V_{rot}$ and 20 kpc nearest-neighbor constraints imposed. Blue diamonds indicate co-rotation, red crosses indicate anti-rotation, and grey circles indicate cases where either is possible due to a combination of orientation and velocity uncertainties. The size of each point is scaled to reflect the EW of the absorber. Concentric rings indicate distances of 1, 2, 3 and 4 R_{vir}. All galaxies are rotated to PA = 90 or 270, such that their major axis' are horizontal and their approaching side is on the left as indicated.

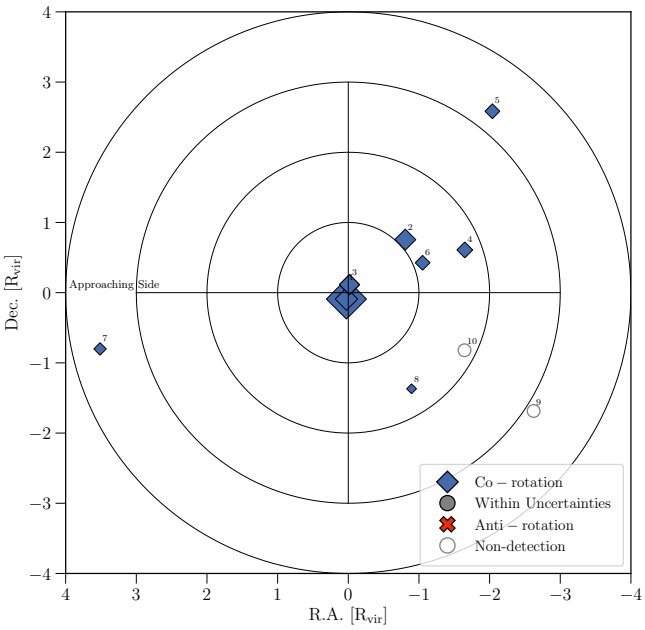

Figure 6. A map of the locations of each absorber normalized with respect to the galaxy virial radius. The color and style of each point indicates the NFW rotation model results for each absorber with $V_{Ly\alpha} \leq V_{rot}$ and $[L^* > 0.5]$ constraints imposed. Blue diamonds indicate co-rotation, red crosses indicate anti-rotation, and grey circles indicate cases where either is possible due to a combination of orientation and velocity uncertainties. The size of each point is scaled to reflect the EW of the absorber. Concentric rings indicate distances of 1, 2, 3 and 4 R_{vir}. All galaxies are rotated to PA = 90 or 270, such that their major axis' are horizontal and their approaching side is on the left as indicated.

REFERENCES

Abazajian, K., Adelman-McCarthy, J. K., Agüeros, M. A., et al. 2005, AJ, 129, 1755

Bowen, D. V., Chelouche, D., Jenkins, E. B., et al. 2016, ApJ, 826, 50

Carilli, C. L., van Gorkom, J. H., & Stocke, J. T. 1989, Nature, 338, 134

Corwin, Jr., H. G., Buta, R. J., & de Vaucouleurs, G. 1994, AJ, 108, 2128

Côté, S., Wyse, R. F. G., Carignan, C., Freeman, K. C., & Broadhurst, T. 2005, ApJ, 618, 178

Danovich, M., Dekel, A., Hahn, O., & Teyssier, R. 2012, MNRAS, 422, 1732

de Blok, W. J. G., Walter, F., Brinks, E., et al. 2008, AJ, 136, 2648

di Nella, H., Paturel, G., Walsh, A. J., et al. 1996, A&AS, 118, 311

Diamond-Stanic, A. M., Coil, A. L., Moustakas, J., et al. 2016, ApJ, 824, 24

Dicaire, I., Carignan, C., Amram, P., et al. 2008, MNRAS, 385, 553

Falco, E. E., Kurtz, M. J., Geller, M. J., et al. 1999, PASP, 111, 438

French, D. M., & Wakker, B. P. 2017, ApJ, 837, 138

Giovanelli, R., Avera, E., & Karachentsev, I. D. 1997, AJ, 114, 122

Green, J. C., Froning, C. S., Osterman, S., et al. 2012, ApJ, 744, 60

Grogin, N. A., Geller, M. J., & Huchra, J. P. 1998, ApJS, 119, 277

Jones, D. H., Read, M. A., Saunders, W., et al. 2009, MNRAS, 399, 683

Keeney, B. A., Momjian, E., Stocke, J. T., Carilli, C. L., & Tumlinson, J. 2005, ApJ, 622, 267

Koribalski, B. S., Staveley-Smith, L., Kilborn, V. A., et al. 2004, AJ, 128, 16

Lu, N. Y., Hoffman, G. L., Groff, T., Roos, T., & Lamphier, C. 1993, ApJS, 88, 383

Lutz, K. A., Kilborn, V. A., Koribalski, B. S., et al. 2018, MNRAS, 476, 3744

Mathewson, D. S., & Ford, V. L. 1996, ApJS, 107, 97

Navarro, J. F., Frenk, C. S., & White, S. D. M. 1996, ApJ, 462, 563

—. 1997, ApJ, 490, 493

Rhee, M.-H., & van Albada, T. S. 1996, A&AS, 115, 407

Rubin, V. C., Thonnard, N. T., & Ford, Jr., W. K. 1982, AJ, 87, 477

Shen, S., Madau, P., Guedes, J., et al. 2013, ApJ, 765, 89

Sofue, Y. 1996, ApJ, 458, 120

Stewart, K. R., Brooks, A. M., Bullock, J. S., et al. 2013, ApJ, 769, 74

Stewart, K. R., Kaufmann, T., Bullock, J. S., et al. 2011, ApJ, 738, 39

Stocke, J. T., Keeney, B. A., & Danforth, C. W. 2010, PASA, 27, 256

Swaters, R. A., Sancisi, R., van Albada, T. S., & van der Hulst, J. M. 2009, A&A, 493, 871

Verheijen, M. A. W., & Sancisi, R. 2001, A&A, 370, 765

Wakker, B. P., Hernandez, A. K., French, D. M., et al. 2015, ApJ, 814, 40

Wakker, B. P., & Savage, B. D. 2009, ApJS, 182, 378

Yim, K., Wong, T., Xue, R., et al. 2014, AJ, 148, 127

APPENDIX

A. ROTATION CURVES

Here we present rotation curves with finder charts indicating the slit position for each galaxy observed with SALT.

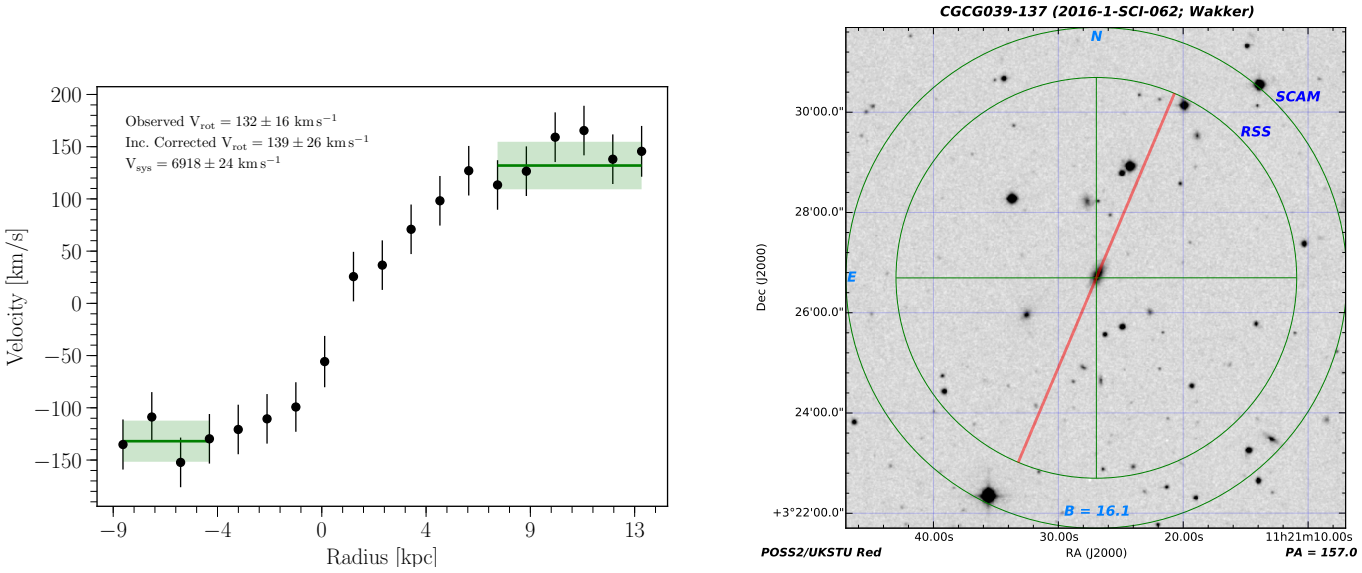

(a) (b)

Figure 7. a) Rotation curve of CGCG039-137. The solid green line indicates the weighted mean velocity over the corresponding x-axis region, and the shaded green indicates the 1σ error in the mean. b) SALT finder chart for CGCG039-137 showing the position of the slit in red.

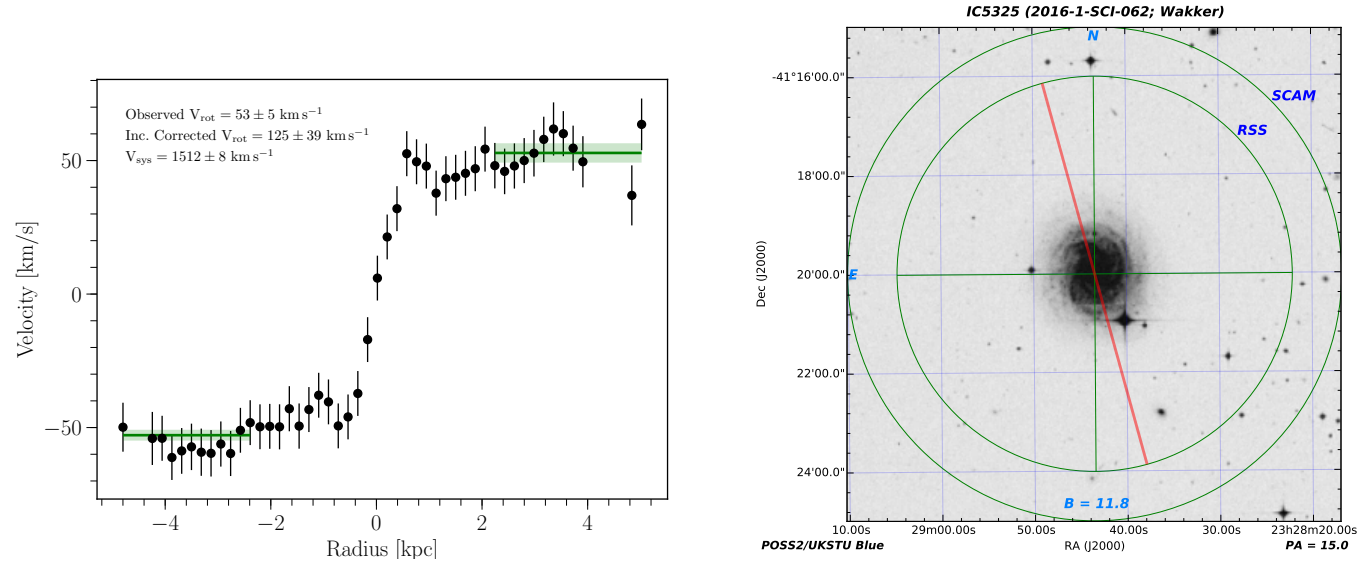

(a) (b)

Figure 8. a) Rotation curve of IC5325. The solid green line indicates the weighted mean velocity over the corresponding x-axis region, and the shaded green indicates the 1σ error in the mean. b) SALT finder chart for IC5325 showing the position of the slit in red.

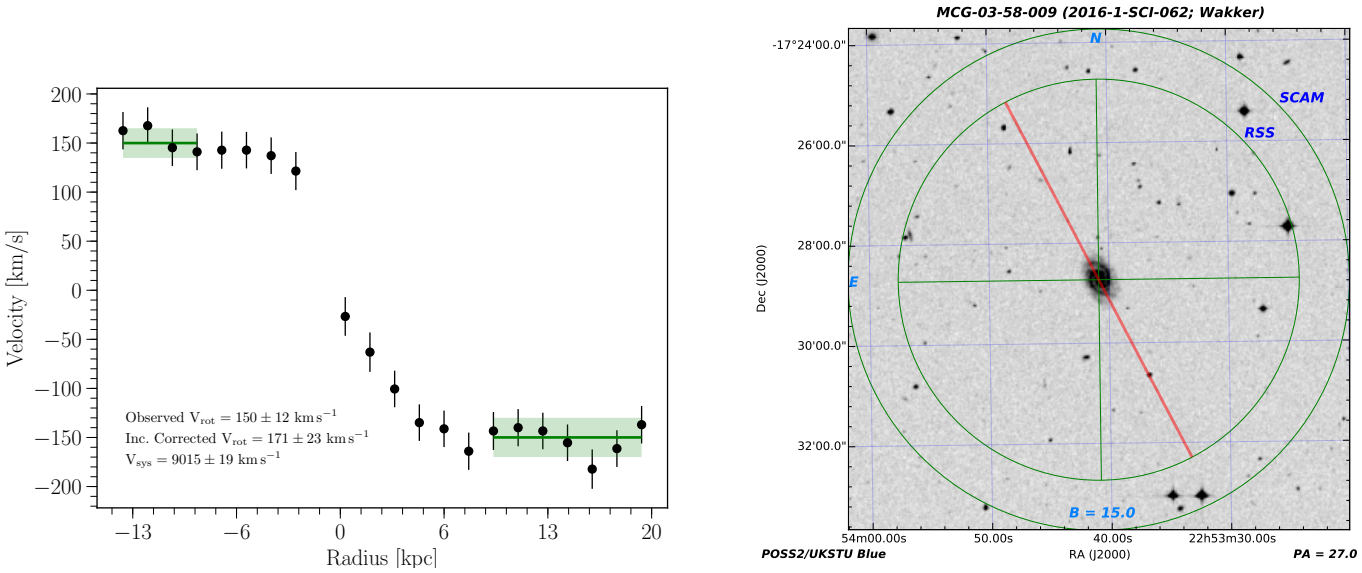

(a) (b)

Figure 9. a) Rotation curve of MCG-03-58-009. The solid green line indicates the weighted mean velocity over the corresponding x-axis region, and the shaded green indicates the 1σ error in the mean. b) SALT finder chart for MCG-03-58-009 showing the position of the slit in red.

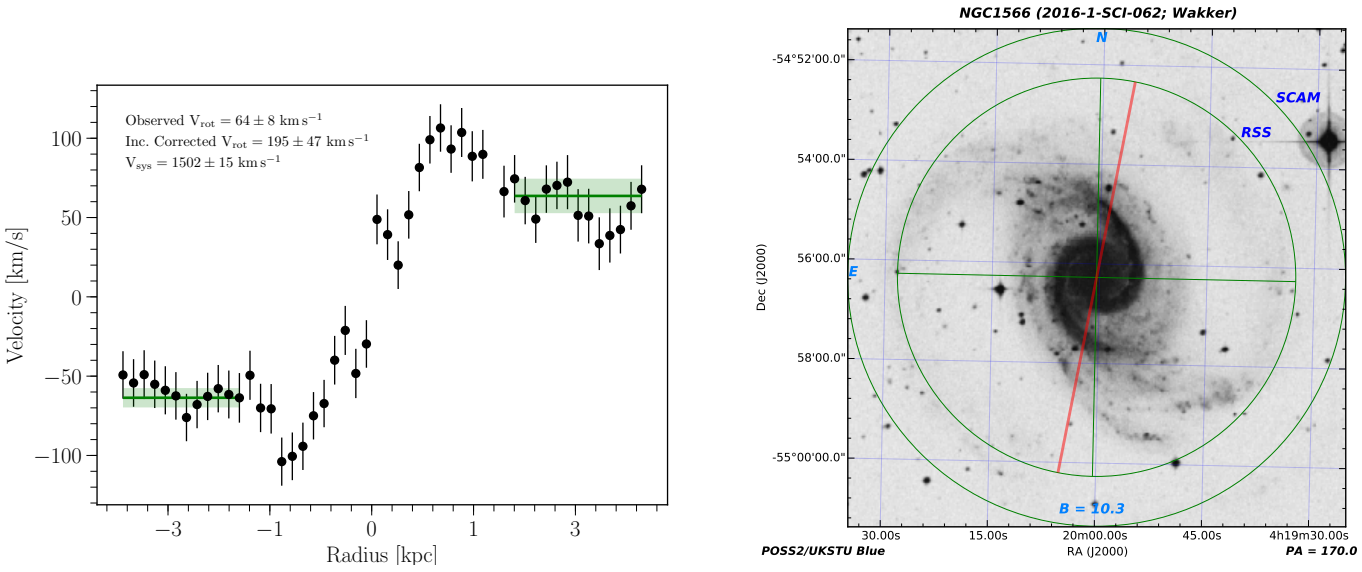

(a) (b)

Figure 10. a) Rotation curve of NGC1566. The solid green line indicates the weighted mean velocity over the corresponding x-axis region, and the shaded green indicates the 1σ error in the mean. b) SALT finder chart for NGC1566 showing the position of the slit in red.

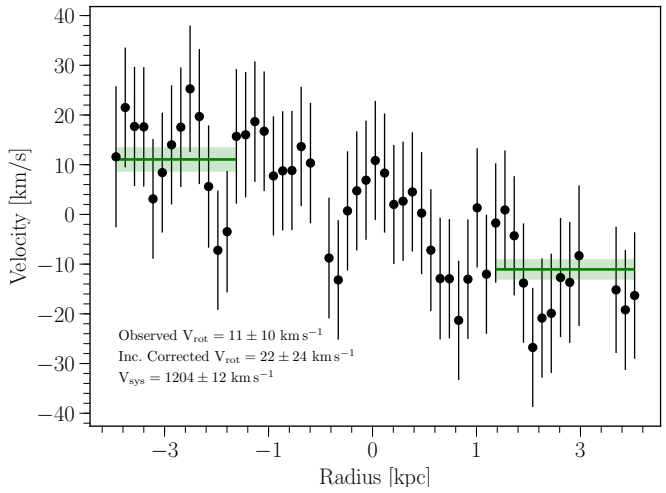

(a)

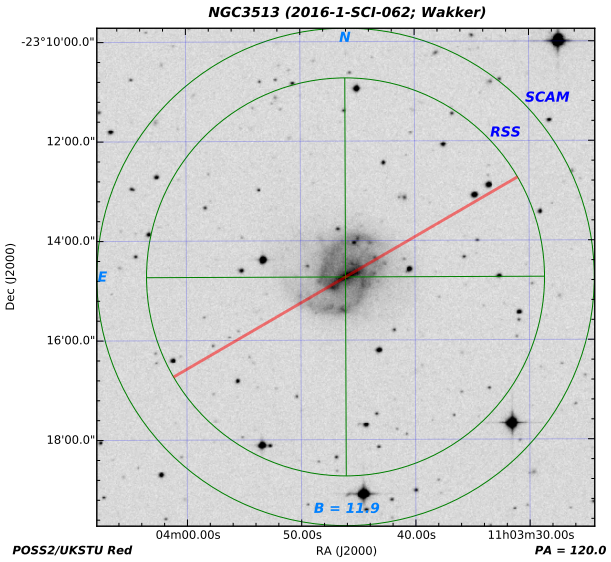

(b)

Figure 11. a) Rotation curve of NGC3513. The solid green line indicates the weighted mean velocity over the corresponding x-axis region, and the shaded green indicates the 1σ error in the mean. b) SALT finder chart for NGC3513 showing the position of the slit in red.

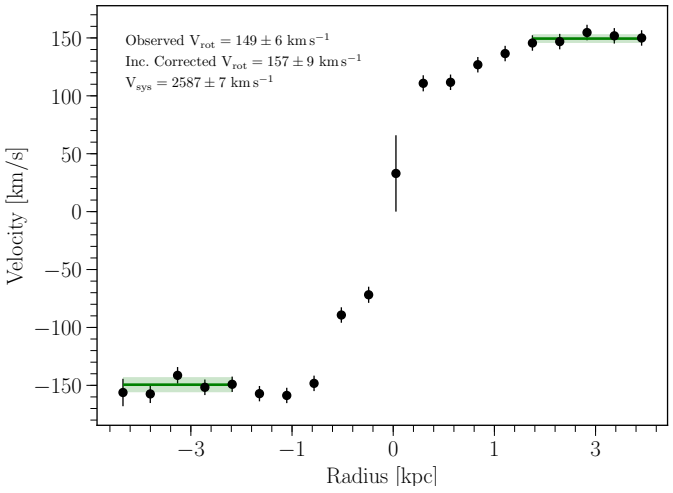

(a)

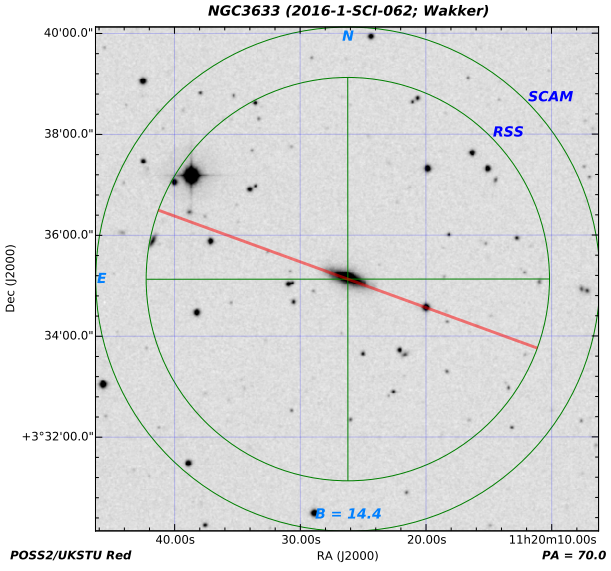

(b)

Figure 12. a) Rotation curve of NGC4536. The solid green line indicates the weighted mean velocity over the corresponding x-axis region, and the shaded green indicates the 1σ error in the mean. b) SALT finder chart for NGC3633 showing the position of the slit in red.

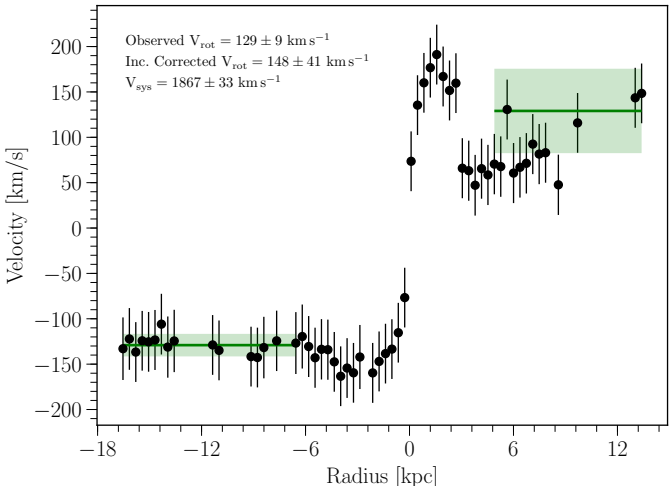

(a)

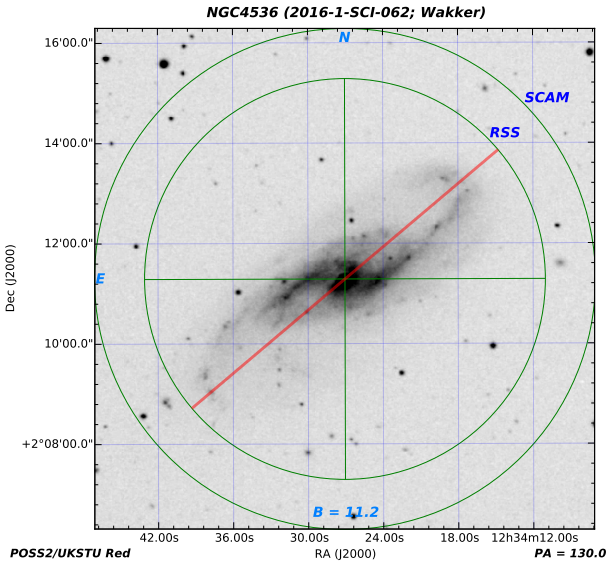

(b)

Figure 13. a) Rotation curve of NGC4536. The solid green line indicates the weighted mean velocity over the corresponding x-axis region, and the shaded green indicates the 1σ error in the mean. b) SALT finder chart for NGC4536 showing the position of the slit in red.

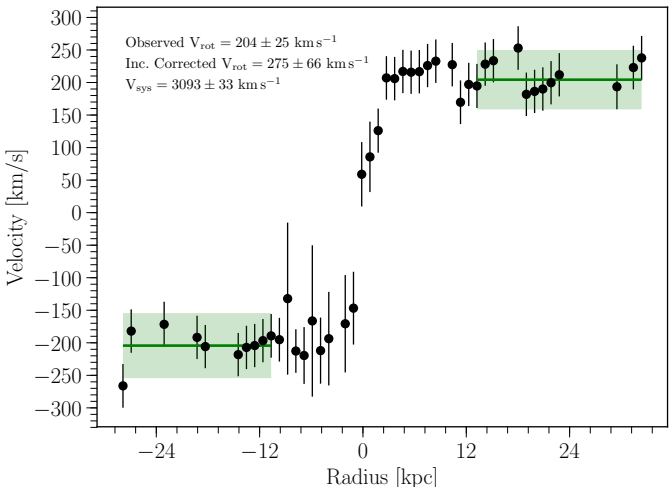

(a)

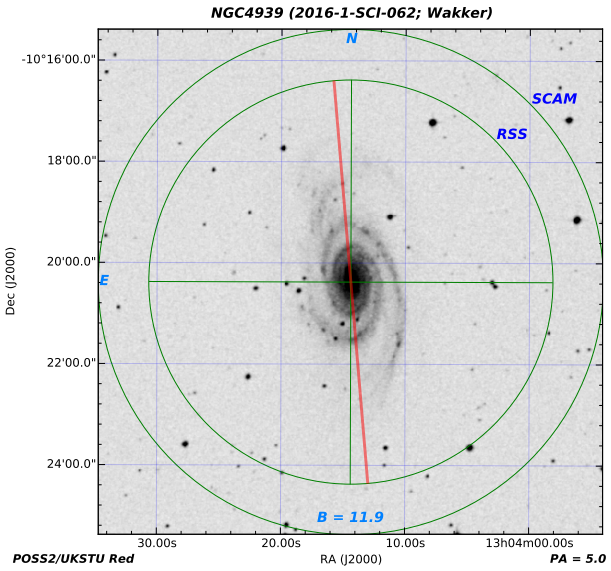

(b)

Figure 14. a) Rotation curve of NGC4939. The solid green line indicates the weighted mean velocity over the corresponding x-axis region, and the shaded green indicates the 1σ error in the mean. b) SALT finder chart for NGC4939 showing the position of the slit in red.

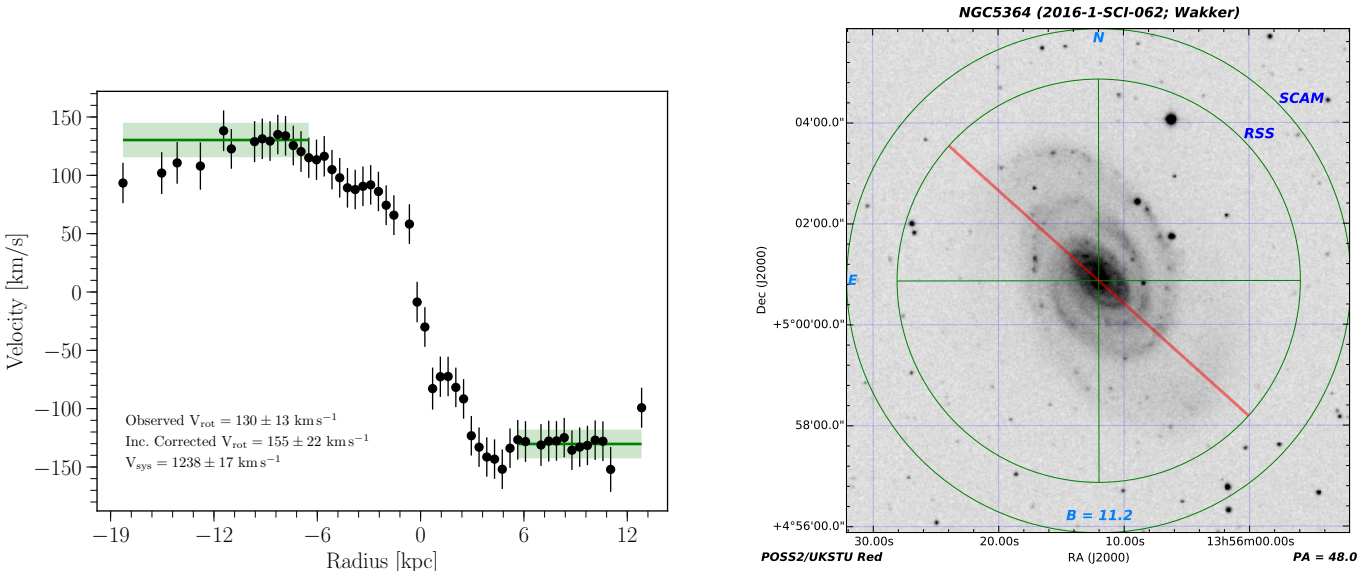

(a) (b)

Figure 15. a) Rotation curve of NGC5364. The solid green line indicates the weighted mean velocity over the corresponding x-axis region, and the shaded green indicates the 1σ error in the mean. b) SALT finder chart for NGC5364 showing the position of the slit in red.

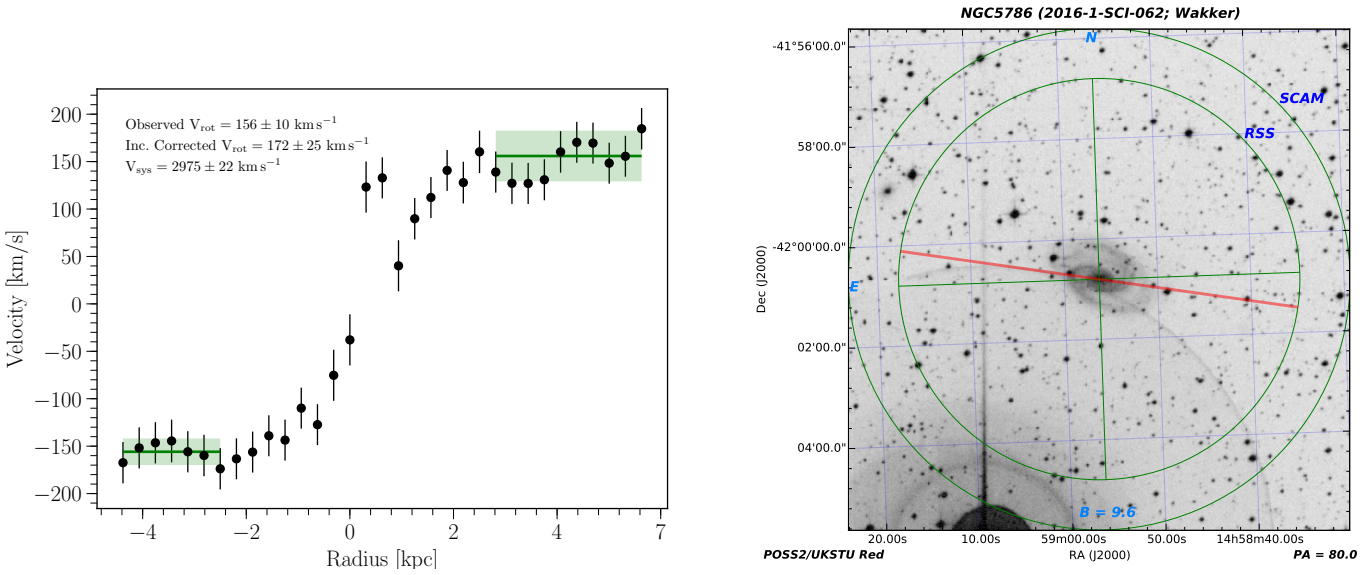

(a) (b)

Figure 16. a) Rotation curve of NGC5786. The solid green line indicates the weighted mean velocity over the corresponding x-axis region, and the shaded green indicates the 1σ error in the mean. b) SALT finder chart for NGC5786 showing the position of the slit in red.

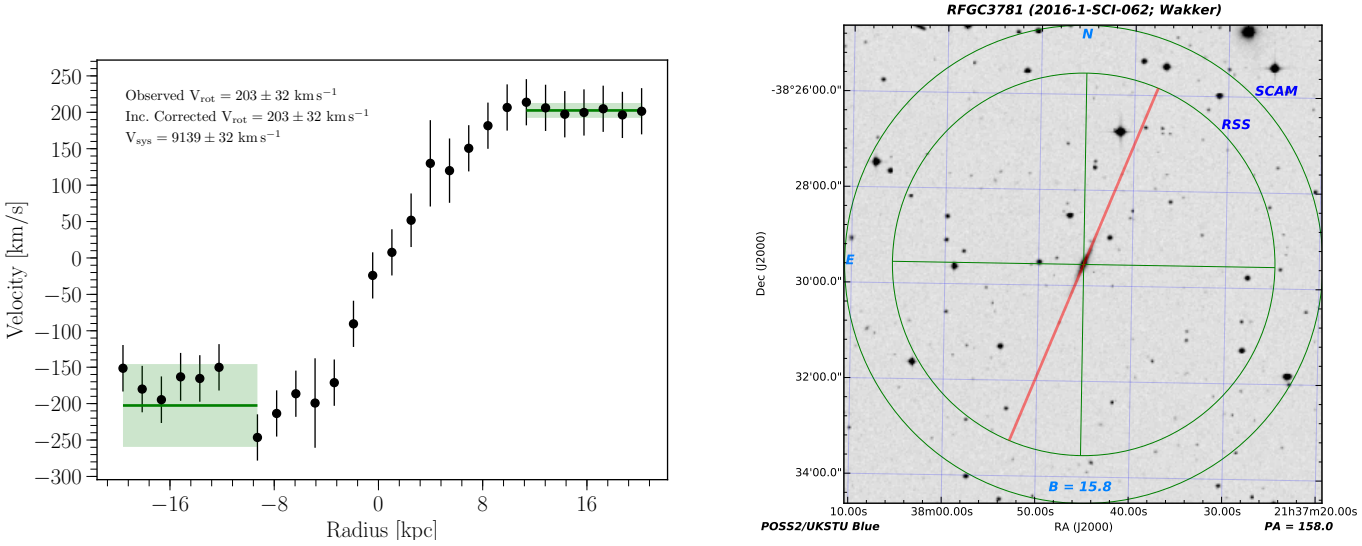

(a) (b)

Figure 17. a) Rotation curve of NGC5364. The solid green line indicates the weighted mean velocity over the corresponding x-axis region, and the shaded green indicates the 1σ error in the mean. b) SALT finder chart for NGC5364 showing the position of the slit in red.